iScience

CellPress
OPEN ACCESS

Article

Ligands with different dimeric configurations potently activate the EphA2 receptor and reveal its potential for biased signaling

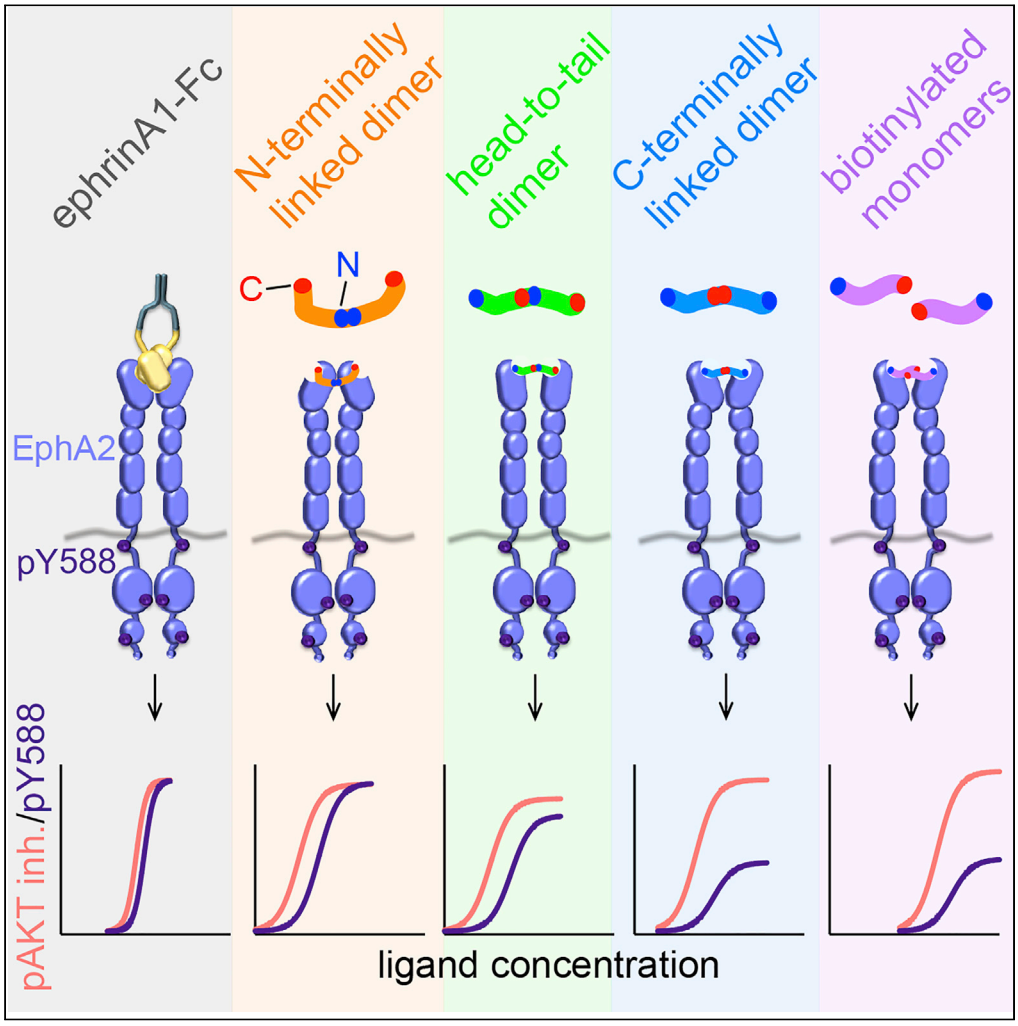

Maricel Gomez-Soler, Marina P. Gehring, Bernhard C. Lechtenberg, ..., Mike W. Matsumoto, Kalina Hristova, Elena B. Pasquale

elenap@sbpdiscovery.org

Highlights

Monomeric peptides were linked to form dimers with distinct geometric configurations

All dimeric peptides activate the EphA2 receptor, some with subnanomolar potency

Distinct ligands differentially regulate two EphA2 signaling responses

The flexible juxtamembrane segment is critical for EphA2 autophosphorylation

Gomez-Soler et al., iScience *25*, 103870
March 18, 2022
https://doi.org/10.1016/j.isci.2022.103870

iScience

CellPress
OPEN ACCESS

Article

Ligands with different dimeric configurations potently activate the EphA2 receptor and reveal its potential for biased signaling

Maricel Gomez-Soler,[1,4] Marina P. Gehring,[1,4] Bernhard C. Lechtenberg,[2] Elmer Zapata-Mercado,[3] Alyssa Ruelos,[1] Mike W. Matsumoto,[1] Kalina Hristova,[3] and Elena B. Pasquale[1,5,*]

SUMMARY

The EphA2 receptor tyrosine kinase activates signaling pathways with different, and sometimes opposite, effects in cancer and other pathologies. Thus, highly specific and potent biased ligands that differentially control EphA2 signaling responses could be therapeutically valuable. Here, we use EphA2-specific monomeric peptides to engineer dimeric ligands with three different geometric configurations to combine a potential ability to differentially modulate EphA2 signaling responses with the high potency and prolonged receptor residence time characteristic of dimeric ligands. The different dimeric peptides readily induce EphA2 clustering, autophosphorylation and signaling, the best with subnanomolar potency. Yet, there are differences in two EphA2 signaling responses induced by peptides with different configurations, which exhibit distinct potency and efficacy. The peptides bias signaling when compared with the ephrinA1-Fc ligand and do so via different mechanisms. These findings provide insights into Eph receptor signaling, and proof-of-principle that different Eph signaling responses can be distinctly modulated.

INTRODUCTION

EphA2 is a receptor tyrosine kinase that belongs to the large Eph receptor family (Pasquale, 2005). Under physiological conditions, EphA2 is predominantly expressed in epithelial and endothelial cell types, where it regulates the integrity of cell-cell junctions and other key properties (Harada et al., 2015; Lin et al., 2010; Miura et al., 2009; Porazinski et al., 2016; Wakayama et al., 2011; Wilson et al., 2021). Given the increased EphA2 expression and/or functional involvement of diverse EphA2 downstream signaling pathways in many cancers (Barquilla and Pasquale, 2015; Pasquale, 2010; Wilson et al., 2021), pathological forms of angiogenesis (Brantley-Sieders et al., 2004; Cheng et al., 2002; Ogawa et al., 2000; Pandey et al., 1995; Zhou et al., 2011), inflammation (Coulthard et al., 2012; Finney et al., 2017; Funk and Orr, 2013; Pandey et al., 1995) and diseases such as cataracts (Cheng et al., 2013; Park et al., 2012; Shiels et al., 2008; Zhang et al., 2009), psoriasis (Gordon et al., 2013) and parasite infections (Barquilla and Pasquale, 2015; Gomez-Soler and Pasquale, 2021), EphA2 has emerged as a potentially important therapeutic target (Barquilla and Pasquale, 2015; Biao-Xue et al., 2011; Gomez-Soler and Pasquale, 2021; Lodola et al., 2017; Pasquale, 2010; Tandon et al., 2011; Wilson et al., 2021).

Various domains in EphA2 can be targeted to modulate its expression and activity (Barquilla and Pasquale, 2015). The extracellular region of EphA2 contains an N-terminal ligand-binding domain (LBD), a cysteine-rich region and two fibronectin type III domains (Himanen et al., 2010; Seiradake et al., 2010) (Figure S1). The intracellular region of EphA2 contains a juxtamembrane segment, the tyrosine kinase domain, a sterile alpha motif (SAM) domain and a short C-terminal tail (Pasquale, 2005). A variety of agents are under investigation to activate or inhibit EphA2 for research and medical applications, including recombinant forms of ephrinA or EphA extracellular regions, antibodies, peptides, small molecule kinase inhibitors, and RNA/DNA oligonucleotides (Barquilla and Pasquale, 2015; Boyd et al., 2014; Gomez-Soler and Pasquale, 2021). Peptides are particularly attractive for EphA2 targeting. They are well suited to bind the broad and shallow ephrin-binding pocket located in the Eph receptor LBD (Figure S1), which is easily accessible on the cell surface (Duggineni et al., 2013; Gambini et al., 2018; Gomez-Soler et al., 2019; Lamberto et al., 2014; Mudd et al., 2020; Riedl and Pasquale, 2015; Salem et al., 2018). In addition, peptides can be used to

[1]Cancer Center, Sanford Burnham Prebys Medical Discovery Institute, La Jolla, CA 92037, USA

[2]Ubiquitin Signalling Division, The Walter and Eliza Hall Institute of Medical Research, Parkville Victoria 3052, Australia and Department of Medical Biology, The University of Melbourne, Parkville, Victoria 3010, Australia

[3]Department of Materials Science and Engineering, Johns Hopkins University, Baltimore, MD 21218, USA

[4]These authors contributed equally

[5]Lead contact

*Correspondence: elenap@sbpdiscovery.org

https://doi.org/10.1016/j.isci.2022.103870

specifically activate or inhibit EphA2 signaling without affecting signaling by other Eph receptors (Gomez-Soler et al., 2019; Koolpe et al., 2002; Riedl and Pasquale, 2015).

EphA2 can assemble into distinct oligomeric structures in response to different ligands (Light et al., 2021; Singh et al., 2018). We reasoned that such different EphA2 assemblies could differentially affect, or bias, signaling responses (Karl et al., 2020). To investigate this possibility, we engineered different dimeric versions of monomeric peptides previously shown to target the ephrin-binding pocket of EphA2 with high selectivity, unlike the highly promiscuous physiological ephrin ligands (Gomez-Soler et al., 2019; Koolpe et al., 2002). We hypothesized that the different types of peptide dimers would stabilize different arrangements of the LBDs in the EphA2 oligomers (including dimers and higher order oligomers), possibly affecting receptor activation and signaling responses. We thus investigated if dimeric peptide ligands with distinct configurations can activate EphA2 and induce the same or different signaling responses. Some of the dimeric peptides we describe here have subnanomolar potency and represent, to our knowledge, the most potent EphA2 agonists reported to date. Indeed, the bivalent binding interactions of dimeric ligands slow down dissociation from the receptor, increasing the apparent binding affinity (avidity) and the receptor residence time of the ligand (Vauquelin and Charlton, 2013).

The availability of a large repertoire of EphA2 activating ligands—including the collection of dimeric peptides described here, dimeric ephrinA1-Fc, monomeric peptides and monomeric ephrinA1 (m-ephrinA1)—allowed us to systematically study whether EphA2 signaling responses can be differentially regulated, or biased, depending on the activating ligand. Ligand bias, also known as ligand functional selectivity, has been extensively studied for G protein-coupled receptors (GPCRs), where it is revolutionizing therapeutic strategies (Kenakin, 2019; Kenakin and Christopoulos, 2013). Ligand bias occurs when two ligands differentially activate distinct receptor signaling responses (Karl et al., 2020; Kenakin and Christopoulos, 2013; Onaran et al., 2017; Smith et al., 2018). There is some evidence that ligand bias can also occur for receptor tyrosine kinases (Trenker and Jura, 2020; Watson et al., 2014; Wilson et al., 2009), but this has not yet been widely explored. Here we present evidence that the EphA2 receptor is potentially capable of biased signaling. We found that distinct ligands can differentially modulate two EphA2 signaling responses. The first is autophosphorylation on tyrosine 588 (Y588), which reports on EphA2 activation and mediates the binding of SH2 domain-containing signaling effectors such as Vav guanine nucleotide exchange factors leading to Rac1 activation and downstream signaling (Barquilla and Pasquale, 2015; Boyd et al., 2014; Fang et al., 2008; Pasquale, 2010). The second is inhibition of AKT S473 phosphorylation, which reports on AKT activation and appears to occur independently of Y588 phosphorylation (Alves et al., 2018; Miao et al., 2009; Yang et al., 2011) (Figure S1). The very high potencies of the peptides, combined with their ability to differentially modulate EphA2 signaling, are highly desirable for therapeutic development (Copeland et al., 2006; Schuetz et al., 2017; Tonge, 2018).

RESULTS

Engineering potent and selective dimeric peptides with different configurations

We previously found that ligands that promote EphA2 dimerization through the "dimerization" interface (Figure S1), which was identified in crystal structures of the EphA2 extracellular region (Himanen et al., 2010; Seiradake et al., 2010), activate EphA2 kinase-dependent signaling (Gomez-Soler et al., 2019; Singh et al., 2018). *In silico* modeling enabled us to design dimeric ligands predicted to induce EphA2 LBD dimerization through this interface by linking previously identified EphA2-targeting peptides through their C-termini (Gomez-Soler et al., 2019) (Figure S2A). Dimer (**1**) was generated from the previously published monomer (**9***) and dimers (**2**) and (**3**) were generated from the previously published monomer (**19***), where the asterisk indicates the numbering in (Gomez-Soler et al., 2019) (Figure 1; Tables S1 and S2). We used a C-terminal disulfide linkage in the case of dimers (**1**) and (**2**) and a more stable non-reducible linker in the case of dimer (**3**). In the *in silico* model, dimer (**1**) induces a symmetric EphA2 LBD dimer and occupies a channel formed in the dimerization interface by EphA2 residues Tyr48, Gly131 and Thr132 (Himanen et al., 2010; Seiradake et al., 2010) (Figures S2A and S3). The binding stoichiometry measured in isothermal titration calorimetry (ITC) experiments with the soluble EphA2 LBD confirmed that two EphA2 LBDs bind to each dimeric peptide (Figures 1, S4A, and S4B; Table S3).

ELISAs measuring peptide-dependent inhibition of EphA2-ephrinA5 interaction revealed that the dimeric peptides are 6–40 times more potent than their monomeric precursors. The IC_{50} values of 71 nM for dimer (**1**) compared to 410 nM for monomer (**9***) and of 0.5 nM for dimer (**2**) and 0.77 nM for dimer (**3**) compared to

Identifier number[1]	Name	Sequence[2]	IC_{50} (nM) by ELISA[3]	K_d (nM) by ITC[3]	Etop pY588[4]	EC_{50} pY588 (nM)[4]	Etop pAKT inh[4]	EC_{50} pAKT inh (nM)[4]	β_{lig}[5]
dimers									
1	βA-WLA-YGSGC dimer (C-ter)	βAWLAYPDSVPYGSGC βAWLAYPDSVPYGSGC	71 ± 26 (8)	2,900 ± 1,300 (2) N = 1.7 ± 0.2	0.49 ± 0.06	150 ± 11 (6)	0.90 ± 0.04	39 ± 8 (6)	0.506 ± 0.12
2	βA-WLA-YRPKC dimer (C-ter)	βAWLAYPDSVPYRPKC βAWLAYPDSVPYRPKC	0.50 ± 0.06 (3)	380 ± 80 (2) N = 2.0 ± 0.2	0.50 ± 0.02	5.6 ± 0.6 (8)	0.86 ± 0.03	0.82 ± 0.15 (7)	0.73 ± 0.11
3	Lys-linked dimer (C-ter)	βAWLAYPDSVPYRPKK βAWLAYPDSVPYRPK	0.77 ± 0.02 (3)	nd	0.46 ± 0.02	2.6 ± 0.2 (6)	1.0 ± 0.03	0.42 ± 0.06 (6)	0.79 ± 0.09
4	CGA-WLA-YR dimer (N-ter)	CGAWLAYPDSVPYR CGAWLAYPDSVPYR	7.9 ± 1.9 (4)	104 ± 1 (2) N = 2.0 ± 0	0.94 ± 0.07	3.5 ± 0.2 (6)	0.90 ± 0.02	0.53 ± 0.08 (6)	0.47 ± 0.10
5	CGA-WLA-YRPK dimer (N-ter)	CGAWLAYPDSVPYRPK CGAWLAYPDSVPYRPK	0.65 ± 0.28 (9)	21 ± 3 (2) N = 2.2 ± 0.2	0.87 ± 0.04	0.75 ± 0.07 (6)	1.0 ± 0.04	0.09 ± 0.02 (6)	066 ± 0.12
6	CGA-WLA-YRPKam dimer (N-ter)	CGAWLAYPDSVPYRPKam CGAWLAYPDSVPYRPKam	0.40 ± 0.10 (5)	nd	0.98 ± 0.08	0.55 ± 0.06 (6)	0.97 ± 0.03	0.08 ± 0.02 (6)	0.51 ± 0.13
7	click dimer (N-ter)	K_{N3}AWLAYPDSVPYRPKam PraGAWLAYPDSVPYRPKam	0.54 ± 0.09 (4)	nd	0.98 ± 0.05	0.64 ± 0.05 (8)	0.87 ± 0.02	0.08 ± 0.01 (8)	0.50 ± 0.10
8	linear dimer (head-to-tail)	βAWLAYPDSVPYRPKG- -GAWLAYPDSVPYRPKam	0.40 ± 0.07 (4)	nd	0.76 ± 0.05	0.73 ± 0.06 (6)	0.87 ± 0.02	0.09 ± 0.01 (6)	0.62 ± 0.09
	ephrinA1-Fc		nd	nd	1.00 ± 0.06	3.8 ± 0.2 (14)	1.0 ± 0.01	1.7 ± 0.2 (14)	0.00
monomers									
	m-ephrinA1		21 ± 8 (3)	nd	0.36 ± 0.03	74 ± 6 (14)	1.0 ± 0.02	27 ± 2 (14)	0.54 ± 0.08
9	CcamGA-WLA-YR	CcamGAWLAYPDSVPYR	1,400 ± 240 (4)	nd	<0.1	nd	nd	nd	nd
10	CcamGA-WLA-YRPK-bio	CcamGAWLAYPDSVPYRPK-bio	27 ± 7 (4)	80 ± 21 (2) N = 0.8 ± 0.1	0.48 ± 0.02	180 ± 20 (9)	1.06 ± 0.03	42 ± 6 (9)	0.64 ± 0.09
2*	YSA-GSGSK-bio	YSAYPDSVPMMSGSGSK-bio	850 ± 440 (43)	9,800 ± 0 (2)	0.42 ± 0.02	3,900 ± 380 (8)	0.98 ± 0.02	600 ± 82 (6)	0.84 ± 0.09

Figure 1. Dimeric peptides with different configurations and other EphA2 ligands

[1] New peptides are numbered **1** through **10**; peptide (**2***) corresponds to peptide (**2**) in (Gomez-Soler et al., 2019) while other relevant peptides from (Gomez-Soler et al., 2019) are listed in Table S2. Blue indicates C-terminally linked dimers, orange N-terminally linked dimers, green a head-to-tail dimer, and lavender monomers. [2] Cysteines and other residues that were linked to achieve dimerization are in red font; also in red font is the Ccam residue in monomers that replaces the cysteine in the corresponding dimers; residues used as spacers are in gray; am, amidated C-terminus; βA, β-Alanine; bio, biotin; Ccam, carbamidomethyl-cysteine; K_{N3}, azido-lysine; Pra, propargylglycine. [3] Averages ±SD are shown. The number of experiments is indicated in parentheses. N for the ITC experiments is the calculated stoichiometry of EphA2 LBD molecules bound to a peptide molecule. [4] Averages are shown ±SE from multiparameter curve fitting of combined data from all experiments. The number of experiments is indicated in parentheses. inh, inhibition. [5] Calculated according to (Equation 1) in Method Details. See also Tables S1–S3 and Figures S1–S4.

19 nM for monomer (**19***) (Gomez-Soler et al., 2019) (Figures 1, 2A, 2B and Table S2) are consistent with the expected increased binding avidity of dimeric ligands for EphA2 immobilized on the ELISA wells (Vauquelin and Charlton, 2013). On the other hand, the K_d values determined in ITC experiments for dimers (**1**) and (**2**) reflect the affinity of the soluble monomeric EphA2 LBD for one of the two binding sites in the dimeric peptides, which should be largely independent of avidity effects (Figures 1, S4A, S4B and Table S3).

To obtain dimeric ligands with a completely different configuration, we joined peptide monomers through their N-termini. We generated dimer (**4**) from monomer (**15***), dimer (**5**) from monomer (**16***), and dimers (**6**) and (**7**) from monomer (**19***) (Gomez-Soler et al., 2019) (Figure 1; Tables S1 and S2). We used an N-terminal disulfide linkage in the case of dimers (**4**), (**5**) and (**6**) and a more stable non-reducible linkage in the case of dimer (**7**) (Figure 1; Table S1; see Method Details). Dimers (**6**) and (**7**) have an amidated C-terminus to increase binding affinity and prevent the possible interaction of the C-terminal carboxylic acid with a neighboring EphA2 LBD (Gomez-Soler et al., 2019).

ITC experiments confirmed the expected binding stoichiometry of two EphA2 LBDs binding to one N-terminally linked dimer (**4**) or (**5**) (Figures 1, S4C, S4D, and Table S3). *In silico* modeling of the two monomeric peptides used to generate dimer (**5**) in complex with dimeric EphA2 LBDs showed that the peptide N-termini are too far apart (~15 Å) to form a disulfide bond (Figure S2B). Manual adjustments of the model to bring the N-terminal cysteines in close proximity to each other required slight translation and tilting by ~45° of each EphA2 LBD (Figure S2C). In this orientation there are only minor contacts between the two EphA2 LBDs (including contacts involving Lys50, Gly75 and Ser113; Figure S3). This LBD arrangement, which to our knowledge has not been observed in available EphA2 crystal structures, may lead to distinctive signaling. Inhibition of ephrinA5 binding to immobilized EphA2 in ELISAs indicated that the N-terminally linked dimers are 30–140 times more potent than the corresponding monomers, with IC_{50} values of 7.9 nM for dimer (**4**) versus 390 nM for monomer (**15***), 0.65 nM for dimer (**5**) versus 55 nM for monomer (**16***), 0.40 nM for dimer (**6**) and 0.54 nM for

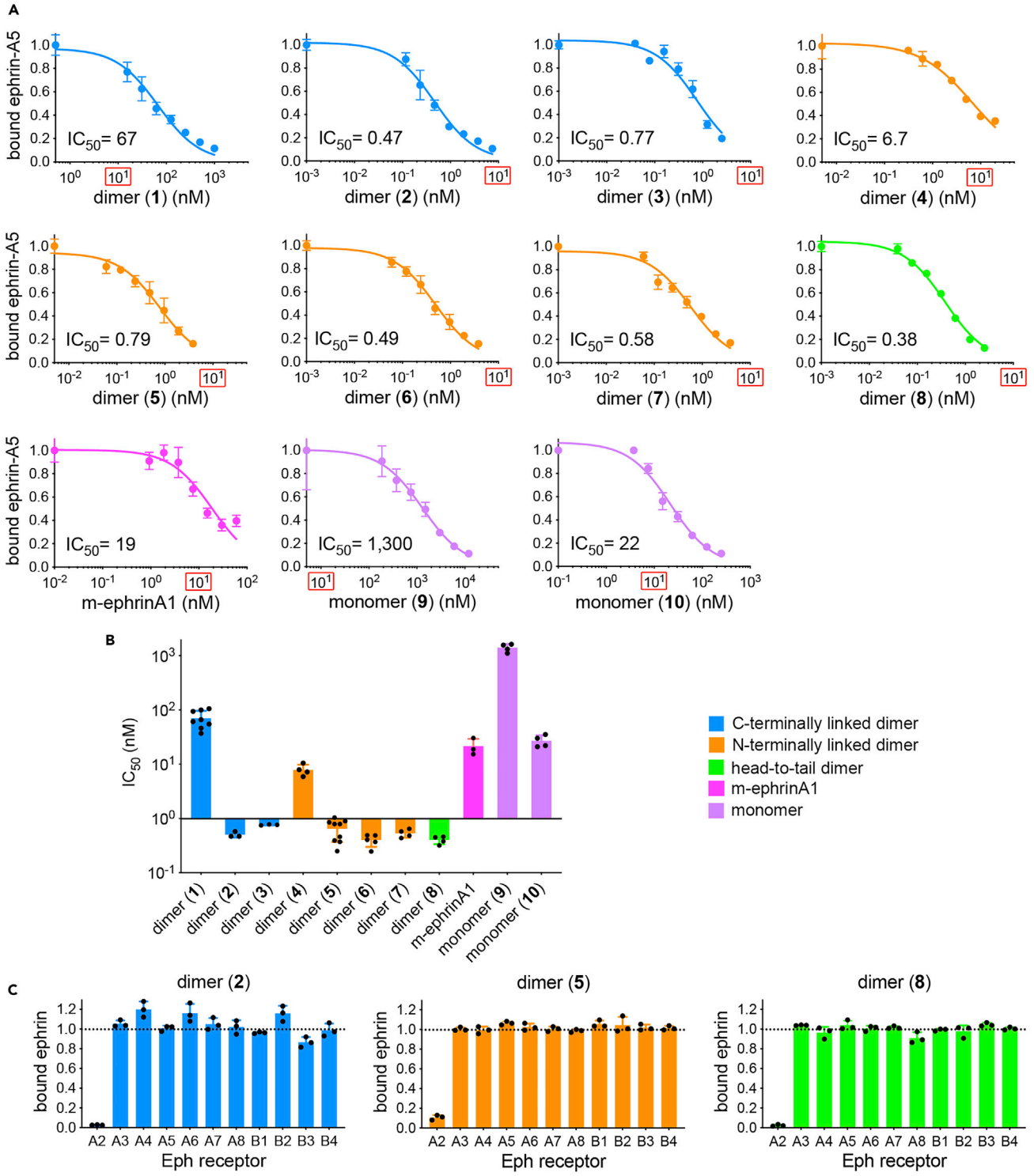

Figure 2. Potency and selectivity of EphA2-targeting dimeric peptides

(A) ELISAs comparing the ability of the peptides to inhibit binding of ephrinA5 fused to alkaline phosphatase (ephrinA5-AP) to the immobilized EphA2 extracellular domain fused to the Fc portion of an antibody (EphA2-Fc). The graphs show averages ±SD from triplicate measurements from a representative experiment and the IC_{50} values calculated from the fitted curves. The 10 nM peptide concentration is outlined in red.

(B) Averages of the IC_{50} values obtained from multiple experiments are shown in panel B (and listed in Figure 1); error bars represent SDs and dots represent the values calculated from individual experiments (n, also reported in Figure 1); a log scale is used for the Y axis.

Figure 2. *Continued*

(C) EphrinA5-AP binding to EphA receptors and ephrinB2-AP binding to EphB receptors in the presence of dimeric peptides representing each of the three configurations. Values are normalized to ephrin binding without peptide. The graphs show averages and SDs from triplicate measurements (with each measurement shown as a dot). The peptides were used at a concentration corresponding to ~100-fold their IC_{50} value: 65 nM for dimer (**2**), 60 nM for dimer (**5**) and 40 nM for dimer (**8**).

dimer (**7**) versus 19 nM for monomer (**19***) (Gomez-Soler et al., 2019) (Figures 1, 2A, and 2B; Table S2). The K_d values measured in ITC experiments with the soluble EphA2 LBD are 104 nM for dimer (**4**) and 21 nM for dimer (**5**) (Figures 1, S4C, and S4D; Table S3), supporting the notion that the subnanomolar potency of the dimers in ELISAs is caused by avidity effects.

To evaluate monomeric peptides more similar in their first three residues to the dimers, we also generated monomers (**9**) and (**10**). These monomers contain an N-terminal carbamidomethylcysteine, which mimics the cysteine present in the dimers but cannot form a disulfide bond, followed by a glycine and an alanine instead of β-alanine (Figure 1; Table S1). Monomers (**9**) and (**10**) are much less potent than the corresponding dimers (**4**) and (**5**) (Figures 1, 2A, 2B and S4E), consistent with the notion that the high potency of the N-terminally linked dimers is due to increased avidity and not to the N-terminal modifications.

To obtain a third dimeric peptide configuration, we designed an asymmetric dimer in which two monomer (**19***) sequences are synthesized one after the other with an intervening GlyGly linker to yield a linear "head-to-tail" dimer (**8**) (Figure 1; Tables S1 and S2). The second peptide sequence starts with alanine instead of β-alanine because protection from digestion by aminopeptidases is not needed for an internal residue. The IC_{50} value for dimer (**8**) in ELISAs is also subnanomolar (Figures 1, 2A, and 2B), again suggesting increased potency because of avidity effects. *In silico* modeling suggests that the two EphA2 LBDs in complex with dimer (**8**) form a symmetric dimer and utilize an interface that partially overlaps with that induced by the C-terminally linked dimer (**1**), including Tyr48, Gly131 and Thr132 (Figures S2D and S3). However, the interface is distinct from the dimerization interface induced by dimer (**1**) because one of the EphA2 LBDs bound to dimer (**8**) is rotated by about 70° and shifted by about 11 Å with respect to the hypothetical plane between the two EphA2 LBDs.

An important feature of the original YSA peptide and its monomeric derivatives is that they specifically bind to EphA2, whereas the ephrinA ligands promiscuously binds to all EphA receptors (Barquilla and Pasquale, 2015; Gomez-Soler et al., 2019; Koolpe et al., 2002; Noberini et al., 2012). Despite their very high potency, dimeric peptides (**2**), (**5**) and (**8**)—representing the three different configurations—are also highly selective for EphA2 and do not bind to other Eph receptors (Figure 2C). Thus, dimers (**1**) through (**8**) represent a collection of very potent and diverse dimeric ligands that are highly specific for EphA2, enabling us to study how differences in ligand configuration, potency and linker type affect EphA2 signaling responses.

Dimeric peptides potently activate EphA2 regardless of their dimeric configuration

To examine the agonistic properties of the different dimeric peptide ligands, we measured EphA2 autophosphorylation on tyrosine 588 (Y588), which is indicative of receptor activation and mediates binding of SH2 domain-containing proteins that link EphA2 to various downstream signaling pathways (Barquilla and Pasquale, 2015; Boyd et al., 2014; Pasquale, 2010) (Figure S1). For these experiments, we stimulated PC3 prostate cancer cells with the dimeric peptides because EphA2 is the prevalent endogenously expressed EphA receptor in these cells (Barquilla et al., 2016), allowing comparisons with the less selective ephrins. Although some prior studies suggest that the orientations of the extracellular and transmembrane regions in receptor tyrosine kinase dimers can affect the arrangement of the intracellular regions with consequences on kinase activity and signaling (Bell et al., 2000; Doerner et al., 2015; Moriki et al., 2001; Sarabipour et al., 2016; Sarabipour and Hristova, 2016), we surprisingly found that peptides with all three different dimeric configurations readily induce robust EphA2 autophosphorylation (Figures 3A–3D). The agonistic potency of the dimers varies according to the potency of their monomeric precursors, as expected, with dimers (**1**) and (**4**) exhibiting 10–60 times lower potency than the other dimers with similar configuration (Figures 1, 3A, and 3D). However, dimers are much more potent than monomers (Figures 1, 3A, 3B, and 3D), likely because of their increased binding avidity for EphA2 on the cell surface. The potency of the dimers also depends on their configuration; the N-terminally linked and head-to-tail dimers exhibit higher potency than the C-terminally linked dimers, with the best EC_{50} values as low as 0.55 to 0.75 nM for dimers (**5**) through (**8**). Another difference that correlates with dimeric configuration is that

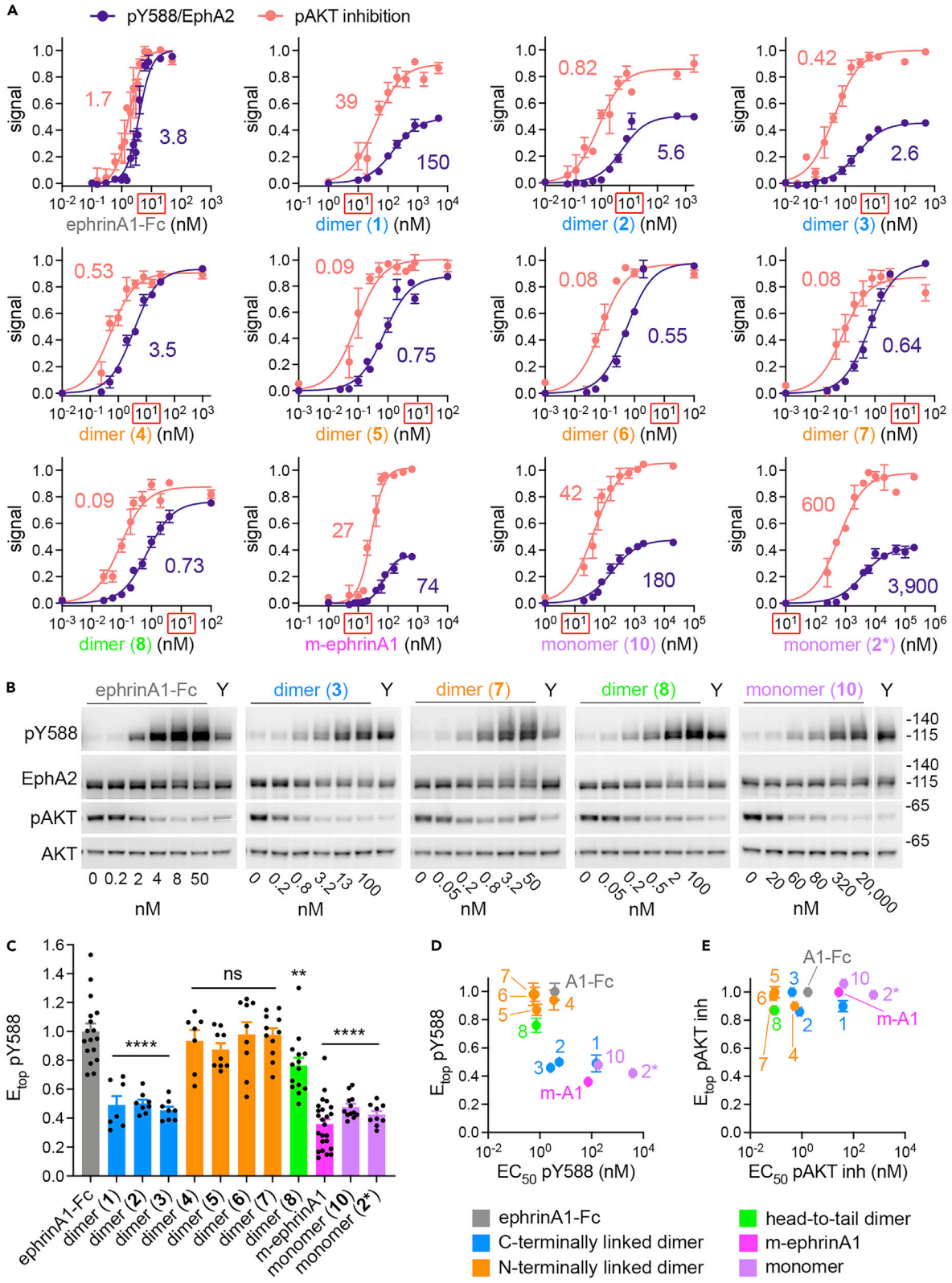
A
pY588/EphA2
pAKT inhibition
signal
1.7
3.8
ephrinA1-Fc (nM)
39
150
dimer (1) (nM)
0.82
5.6
dimer (2) (nM)
0.42
2.6
dimer (3) (nM)
0.53
3.5
dimer (4) (nM)
0.09
0.75
dimer (5) (nM)
0.08
0.55
dimer (6) (nM)
0.08
0.64
dimer (7) (nM)
0.09
0.73
dimer (8) (nM)
27
74
m-ephrinA1 (nM)
42
180
monomer (10) (nM)
600
3,900
monomer (2*) (nM)
B
ephrinA1-Fc
dimer (3)
dimer (7)
dimer (8)
monomer (10)
Y
pY588
EphA2
pAKT
AKT
-140
-115
-65
0 0.2 2 4 8 50
0 0.2 0.8 3.2 13 100
0 0.05 0.2 0.8 3.2 50
0 0.05 0.2 0.5 2 100
0 20 60 80 320 20,000
nM
C
E_top pY588
ns
**
****
****
ephrinA1-Fc
dimer (1)
dimer (2)
dimer (3)
dimer (4)
dimer (5)
dimer (6)
dimer (7)
dimer (8)
m-ephrinA1
monomer (10)
monomer (2*)
D
E_top pY588
EC50 pY588 (nM)
A1-Fc
m-A1
E
E_top pAKT inh
EC50 pAKT inh (nM)
A1-Fc
m-A1
ephrinA1-Fc
C-terminally linked dimer
N-terminally linked dimer
head-to-tail dimer
m-ephrinA1
monomer

Figure 3. Dimeric peptides efficiently promote EphA2 autophosphorylation and downstream signaling

(A) Dose-response curves for EphA2 autophosphorylation on tyrosine 588 (pY588; purple) and for downstream inhibition of AKT phosphorylation (magenta). PC3 cells were treated for 15 min with different concentrations of the indicated peptides. EphA2 pY588 (indicative of receptor activation), total EphA2, AKT phosphorylation on S473 (pAKT, indicative of AKT activation) and total AKT were quantified from immunoblots. pY588/EphA2 values were normalized to the value obtained with saturating ephrinA1-Fc concentration. pAKT inhibition was calculated as 1– pAKT/AKT values normalized to the level in cells not treated with ligand. The graphs show quantifications from multiple blots (averages ±SE; the number of experiments used to generate each curve is shown in Figure 1). EC_{50} values (nM, shown) were calculated by non-linear regression with a Hillslope of 1 for the peptides and of 2 for ephrinA1-Fc and m-ephrinA1; the 10 nM concentration is outlined in red.

(B) Examples of immunoblots of lysates from PC3 cells treated with the indicated concentrations of representative ligands. Y indicates treatment with 100 μM of the previously identified YSA-GSGSK-bio monomer (**2***), which was included in all blots for comparison. A white vertical line indicates removal of irrelevant lanes. Molecular weight markers (in kDa) are indicated on the right.

(C) The highest EphA2 Y588 phosphorylation induced by each ligand (E_{top} pY588) depends on the type of ligand and dimeric configuration. The graphs show the pY588/EphA2 values induced by 15 min stimulation with saturating concentrations of the different ligands normalized to the value for the reference ligand ephrinA1-Fc. The bars show averages ±SE, and the individual measurements are shown as black dots. The asterisks indicate the significance of the difference from ephrinA1-Fc, calculated using one-way ANOVA followed by the Dunnett's multiple comparisons test (**, $p < 0.01$; ****, $p < 0.0001$; ns, not significant).

(D and E) Different ligands cause different E_{top} pY588, EC_{50} pY588 and EC_{50} pAKT inhibition (inh) but similar E_{top} pAKT inh. Plots of E_{top} versus EC_{50} for pY588 in D and for pAKT inh in (E) Averages ±SE are shown for the peptides and ephrinA1. See also Figures S5 and S9.

the three C-terminally linked dimers have lower efficacy (i.e. they induce lower maximal EphA2 Y588 phosphorylation, E_{top} pY588; Figures 1, 3A, 3C, and 3D). In contrast, the nature of the linker used for dimerization does not seem to have major effects on potency.

The engineered ligand most widely used to activate EphA2 signaling is the dimeric ephrinA1-Fc, in which the ephrinA1 extracellular region is fused to the dimeric Fc portion of an antibody. Treatment of cells with ephrinA1-Fc is known to induce EphA2 oligomerization, autophosphorylation on tyrosine residues including Y588, and downstream signaling (Barquilla et al., 2016; Fang et al., 2008; Singh et al., 2018). Remarkably, ephrinA1-Fc (EC_{50} = 3.8 nM) is substantially less potent than peptide dimers (**5**) through (**8**) (Figures 1, 3A, 3B, and 3D).

The monomeric m-ephrinA1 ligand, which is also known to induce EphA2 autophosphorylation, was as expected less potent than ephrinA1-Fc (Beauchamp et al., 2012) (Figures 1, 3A, and 3D). The monomeric CcamGA-WLA-YRPK-bio (**10**) peptide, but not CcamGA-WLA-YR (**9**), also induced EphA2 autophosphorylation (Figures 1 and 3A–3D), in agreement with our previous observation that a C-terminal biotin confers agonistic properties to this class of monomeric peptides (Gomez-Soler et al., 2019). Thus, CcamGA-WLA-YRPK-bio (**10**) represents a monomeric EphA2 agonist with nanomolar potency.

EphA2 activation by ephrinA1-Fc is also known to strongly inhibit AKT in PC3 cells, which can be monitored by measuring the decrease in AKT phosphorylation on S473 (Yang et al., 2011) (Figures 3A, 3B, 3E and S1). We found that all peptide agonists and m-ephrinA1 also inhibit AKT in a concentration-dependent manner (Figures 1 and 3A, 3B, and 3E) (Gomez-Soler et al., 2019). Treatment of PC3 cells with ephrinA1-Fc also induces retraction of the cell periphery and cell rounding, a response related to inhibition of cell migration/invasion (Barquilla et al., 2016). We found that dimeric peptides representing the three different configurations and monomer (**10**) also all induce cell retraction, with a slightly smaller decrease in cell area induced by the dimeric peptides compared to ephrinA1-Fc (Figure S5). Thus, like the ephrins, all peptide agonists can promote not only EphA2 autophosphorylation but also downstream signaling and changes in cell behavior. A difference between the peptides and ephrinA1 is that dose-response curves with a Hill coefficient of 1 satisfactorily describe the data obtained with the peptides but not the data obtained with ephrinA1-Fc and m-ephrinA1, for which a Hill coefficient of 2 yields a much better fit. This suggests positive cooperativity in the binding of both monomeric and dimeric forms of ephrinA1 to EphA2.

The kinetics of EphA2 signaling differ depending on the activating ligand

As mentioned above, EphA2 Y588 phosphorylation levels induced by stimulating PC3 cells for 15 min with saturating ligand concentrations (inducing maximal E_{top} pY588) are lower for the C-terminally linked dimers and the monomeric ligands than for the N-terminally linked dimers and head-to-tail dimer (**8**), which are similar to the reference ligand ephrinA1-Fc (Figures 1, 3C, and 3D), suggesting that the configuration of the dimers affects signaling features. For example, C-terminally linked dimers may be partial agonists that are able to achieve only low maximal EphA2 Y588 phosphorylation. Alternatively, different ligands may regulate EphA2 phosphorylation with distinct kinetics. If the EphA2 phosphorylation kinetics are

slower for C-terminally linked dimers, peak phosphorylation levels may not be reached by 15 min. If the kinetics of dephosphorylation are faster, peak phosphorylation may have already declined by 15 min. To distinguish among these possibilities, and to further characterize the activities of the different ligands, we performed time course experiments with saturating concentrations of peptides representative of each group and ephrinA1-Fc.

The peak of Y588 phosphorylation normalized to EphA2 (pY588/EphA2) induced by all ligands examined occurred after 2.5–10 min of stimulation and the levels were only slightly reduced after 15 min (Figures 4A and S6). This suggests that the configuration of the dimeric peptides does not strongly affect the kinetics of Y588 phosphorylation in the first 15 min of stimulation. Therefore, the C-terminally linked dimers and the monomers are partial agonists that induce lower E_{top} pY588/EphA2 values. pY588/EphA2 levels gradually decreased after 1 to 3 h of stimulation, reflecting receptor dephosphorylation, but were still substantially elevated after 3 h, particularly in the case of the N-terminally linked dimer (**7**).

EphA2 levels, normalized to AKT as a loading control, decreased after prolonged stimulation (Figure 4B), as would be expected because ligand-induced EphA2 activation is followed by internalization and degradation with a slower time course (Walker-Daniels et al., 2002). EphA2 loss was less pronounced for the C-terminally linked dimer (**3**) and monomer (**10**) than for the other ligands, highlighting differences in EphA2 degradation induced by different ligands that may be due to the lower receptor tyrosine phosphorylation levels induced by dimer (**3**) and monomer (**10**) (Figures 1, 3C, and 3D). The amount of EphA2 phosphorylated on Y588 (normalized to AKT as a loading control) persisted at higher levels when induced by dimer (**7**) and monomer (**10**) than by the other ligands (Figure 4C), consistent with the slower receptor dephosphorylation induced by dimer (**7**) and the slower receptor degradation induced by monomer (**10**) (Figures 4A and 4B). Finally, all dimeric peptides similarly reduced AKT phosphorylation to very low levels, with maximal AKT dephosphorylation observed at ~10 min (Figure 4D). AKT phosphorylation then gradually recovered over time, returning to almost the initial level after 3 h of stimulation in the case of all three dimeric peptides. In contrast, AKT phosphorylation remained low (~40% of the initial level) after 3 h of stimulation with ephrinA1-Fc and monomer (**10**). Thus, saturating concentrations of different ligands have distinctive effects on the time course of EphA2 dephosphorylation and degradation and on the persistence of a downstream signaling effect such as inhibition of AKT.

Dimeric peptides with different configurations induce EphA2 oligomers larger than dimers

To examine the effects of dimeric peptide ligands on EphA2 oligomerization (including dimerization and higher order clustering), we performed quantitative FRET experiments in live cells (Gomez-Soler et al., 2019; Singh et al., 2015; Singh et al., 2017a; Singh et al., 2018; Singh et al., 2016). In these experiments, EphA2 molecules tagged at the C-terminus with a donor (mTURQ) or acceptor (EYFP) fluorescent protein are co-expressed in HEK293 cells by transient transfection. FRET is then measured in hundreds of individual cells with different EphA2 expression levels (Figure S7A), and the data are combined to yield average oligomeric fractions at different EphA2 concentrations (Figures 5A–5D). Oligomerization curves for different monomer-oligomer association models are then fitted to the data points to identify the oligomer model that produces the best fit (i.e., the least mean square error (MSE)) (King et al., 2017) (Figure S7B).

In experiments previously performed in the absence of ligand, we found that EphA2 oligomerization is best described by a monomer-dimer model (Gomez-Soler et al., 2019) (Figure 5A). The dissociation constant determined from fitting the dimerization curve for the EphA2 G131Y mutant, which has impaired ability to assemble through the "dimerization" interface, was similar to that for EphA2 wild-type (WT). In contrast, the dissociation constant determined for the EphA2 L223R/L254R/V255R triple mutant, which has impaired ability to assemble through the previously described "clustering" interface (Himanen et al., 2010; Seiradake et al., 2010), was significantly higher than for EphA2 WT, indicating that the mutations impair dimerization (Gomez-Soler et al., 2019). These experiments suggested that unliganded EphA2 forms dimers that are stabilized through the clustering interface.

To obtain the data points for oligomerization curves (Figure S7A), we need to accurately determine the concentration of EphA2 in each small region of plasma membrane in which FRET efficiency is measured. Conversion of fluorescence intensity into accurate 2-dimensional EphA2 concentration requires a reversible hypo-osmotic treatment to swell the cells and smooth the wrinkled topology of their plasma membrane (Gomez-Soler et al., 2019; Singh et al., 2015; Singh et al., 2017a; Singh et al., 2018; Singh et al.,

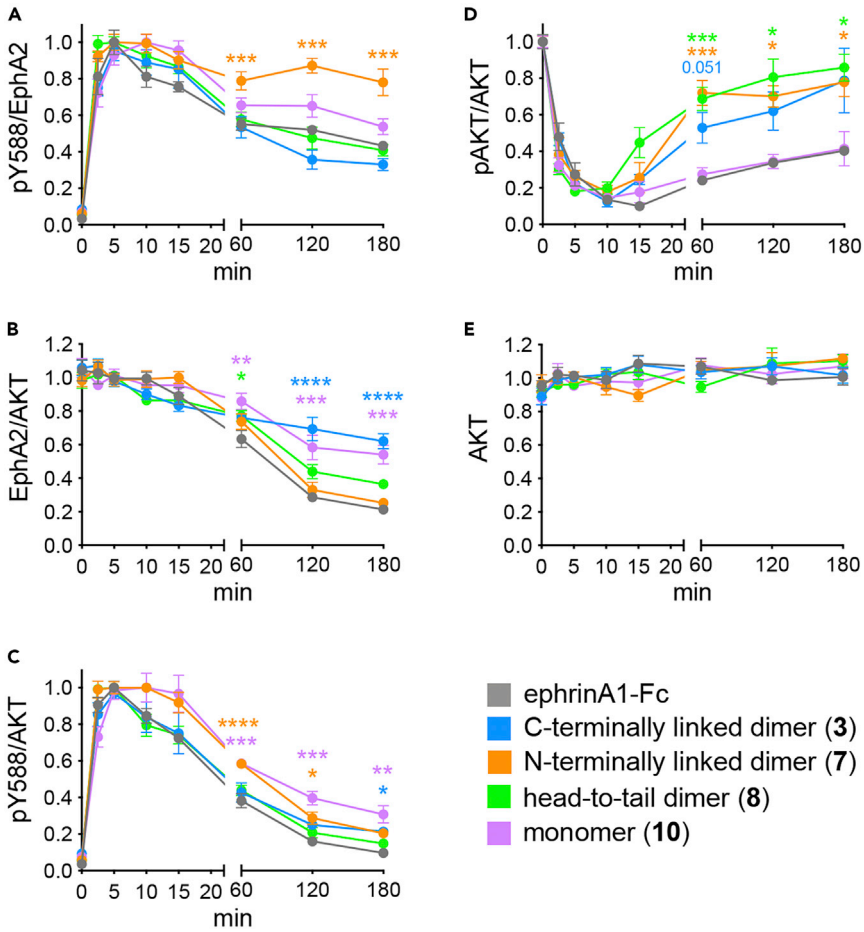

Figure 4. Different EphA2 ligands regulate pY588 phosphorylation and AKT inhibition with distinct kinetics. PC3 cells were treated for the indicated time periods with saturating concentrations of ephrinA1-Fc, the indicated dimeric peptides representative of each configuration, or monomeric peptide (10). Y588 and AKT phosphorylation levels and total EphA2 and AKT levels were quantified from immunoblots of cell lysates

(A) pY588/EphA2, normalized to the peak value.

(B) EphA2/AKT (with AKT used as loading control) normalized to the average of the values at 0, 2.5, 5 and 10 min (when receptor degradation does not yet occur).

(C) pY588/AKT, normalized to the peak value.

(D) pAKT/AKT, normalized to the "0" time point corresponding to no ligand treatment.

(E) AKT values normalized to the average of all the values for each ligand. The graphs show averages ±SE from 3 to 8 independent measurements. The asterisks indicate the significance of the difference from ephrinA1-Fc for the last 3 time points, calculated by mixed-effects analysis followed by the Dunnett's multiple comparisons test (*, $p < 0.05$; **, $p < 0.01$; ***, $p < 0.001$; ****, $p < 0.0001$; $p = 0.051$ is also indicated, with the color of the asterisks indicating which peptide is significantly different from ephrinA1-Fc). See also Figure S6.

2016) (Figure 5E). This process does not cause irreversible cell damage or alter membrane protein interactions in a measurable way (King et al., 2016; Singh et al., 2017b), and EphA2 is uniformly distributed in the plasma membrane of the swollen cells (Figure 5E).

To acquire FRET data, we treated the swollen cells with saturating concentrations of the C-terminally linked dimeric peptide (**2**) and the N-terminally linked dimeric peptide (**5**). This caused the formation of fluorescent patches of EphA2 WT (Figure 5E) similar to those previously observed in response to ephrinA-Fc ligands (Seiradake et al., 2013), which induce EphA2 oligomers that are larger than dimers (Singh et al., 2018). Thus, the patches likely reflect EphA2 clustering. The FRET data in the presence of the two peptide ligands are well described by a higher order oligomer model (Figure 5B, dashed lines, and S7B), corresponding to steeper oligomerization curves than the dimerization curve for EphA2 WT in the absence of

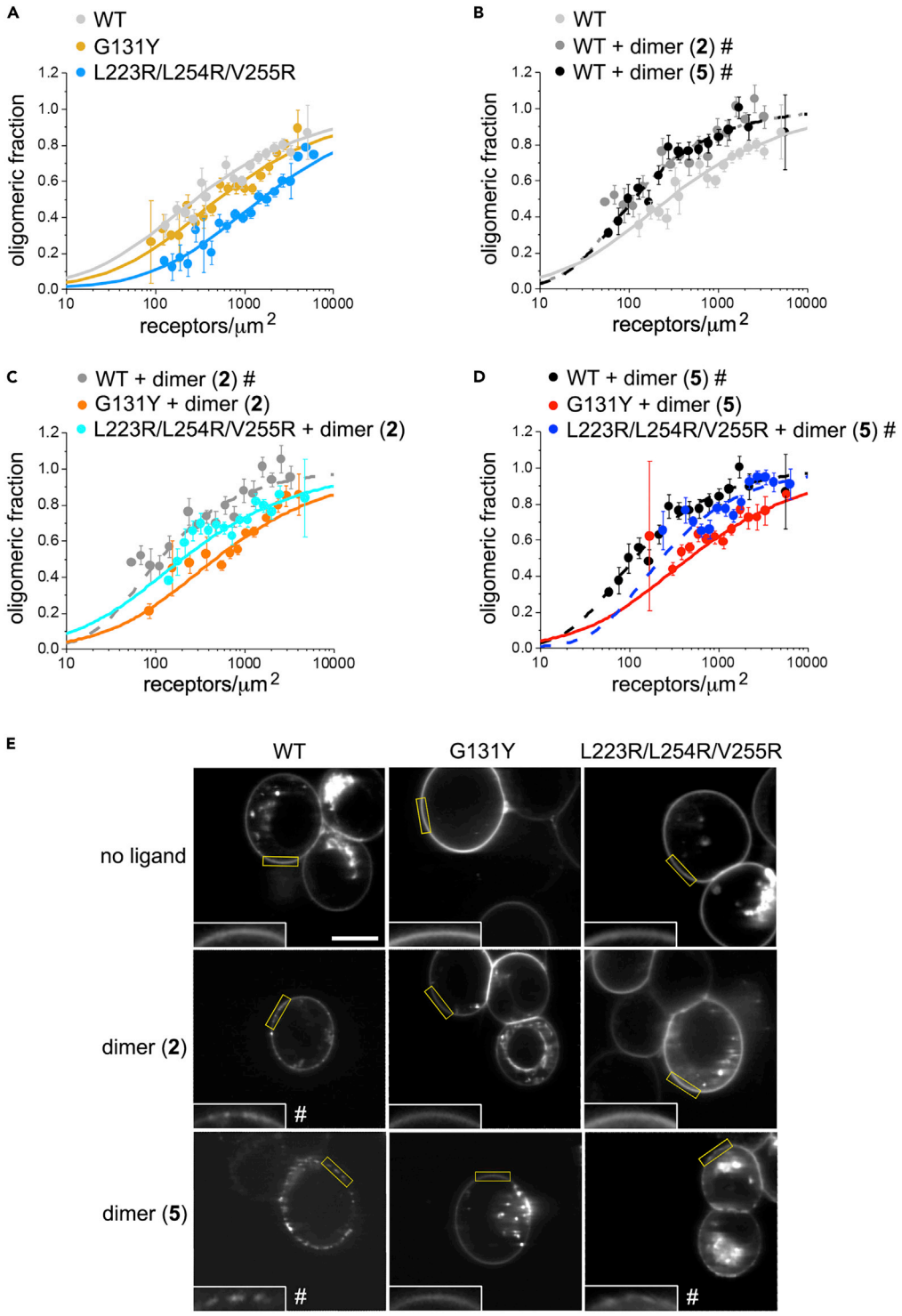

Figure 5. Dimers with different configurations induce EphA2 oligomerization and patching on the cell surface

(A-D) Oligomerization curves comparing EphA2 WT and the G131Y and L223R/L254R/V255R interface mutants transiently expressed in HEK293 cells and treated with saturating concentrations of C-terminally linked dimer (**2**) or N-terminally linked dimer (**5**). The data for EphA2 in the absence of ligand treatment in panels A and B are from (Gomez-Soler et al., 2019), although binned slightly differently for consistency with the other data shown in the figure. The curves were obtained by fitting quantitative FRET data to monomer-oligomer models. Curves derived from best fit monomer-dimer models are shown as solid lines, and curves derived from best fit monomer-higher order oligomer models are shown as

Figure 5. *Continued*

dashed lines. Curves for higher order oligomerization are steeper than dimerization curves. Averages ±SE are shown in the graphs; n values are shown in Figure S7.

(E) Two-photon integrated fluorescence images of HEK293 cells expressing EphA2-EYFP and EphA2-mTURQ and under hypo-osmotic conditions. The plasma membrane regions in the rectangular yellow outlines are enlarged in the insets at the bottom of each panel. The dimeric peptides induce patching of EphA2 WT on the plasma membrane and dimer (**5**) also induces patching of the EphA2 L223R/L254R/V255R mutant, while in the other cases the EphA2 interface mutations disrupt patching. # indicates the presence of EphA2 patches in the plasma membrane. The scale bar represents 10 μm for the main panels and 4 μm for the insets. See also Figure S7.

ligand (Figure 5B, solid line). Interestingly, the oligomerization curves in the presence of the two dimeric peptides are very similar, suggesting that the stabilities of the EphA2 oligomers bound to the two peptides are similar.

The FRET data for the EphA2 G131Y and L223R/L254R/V255R mutants treated with dimeric peptide (**2**) are best described by a dimerization model (Figure 5C, solid lines, and S7B). Consistent with this, these EphA2 mutants do not form patches in the presence of dimer (**2**) (Figure 5E). This suggests that mutations in either interface reduce the EphA2 oligomers to dimers. The data for the EphA2 G131Y mutant in the presence of dimeric peptide (**5**) are also best described by a dimer model (Figure 5D, solid line, and S7B), but the data for the EphA2 L223R/L254R/V255R mutant suggest oligomerization (Figure 5D, dashed line, and S7B). Consistent with these FRET data, dimer (**5**) causes patches of the EphA2 L223R/L254R/V255R mutant but not of the G131Y mutant (Figure 5E). These data suggest that the dimerization interface plays an important role in EphA2 oligomerization in response to dimer (**5**), while the clustering interface is much less involved. This is not surprising because our *in silico* modeling suggests that dimer (**5**) stabilizes the EphA2 LBD dimer through an interface that is different from the clustering interface (Figures S2C and S3).

Taken together, our FRET data are not consistent with a simple EphA2 dimerization model and instead suggest that the dimeric peptides induce larger EphA2 oligomers that utilize different interfaces. The formation of higher order EphA2 oligomers might contribute to the ability of dimeric peptide ligands with different configurations to activate EphA2, by enabling not only cross-phosphorylation within an EphA2 dimer but also phosphorylation by the kinase domain of a neighboring dimer.

The flexible juxtamembrane segment is required for EphA2 autophosphorylation and downstream signaling

In an EphA2 dimer, the 50 amino acid-long flexible juxtamembrane segment (Figure S1) could allow an arrangement of the kinase domains suitable for cross-phosphorylation, independently of the orientation of the LBDs. Reorientation of domains through flexible linkers is supported by some studies with other receptor tyrosine kinases (Lu et al., 2010; Lu et al., 2012; Mi et al., 2011; Sorokin, 1995). To investigate the potential involvement of the juxtamembrane segment in EphA2 activation induced by dimeric peptides, we generated stable HEK293 cells expressing EphA2 WT and two EphA2 mutants: the ΔQ565-L582 mutant lacking 18 juxtamembrane residues (Δjxtm-1) and the ΔQ565-T606 mutant lacking 42 residues, which represent most of the juxtamembrane segment (Δjxtm-2).

Since the major Y588 and Y594 autophosphorylation sites are in the deleted region of the EphA2 Δjxtm-2 mutant, we monitored overall tyrosine phosphorylation as well as phosphorylation of two other major phosphorylation sites still present in the mutants, Y772 in the activation loop of the kinase domain and Y930 in the SAM domain (Figure S1). We found that EphA2 WT is substantially tyrosine phosphorylated in the absence of ligand (WT lanes labeled "–" in the blots in Figures 6A–6D), likely because the elevated expression of the transfected EphA2 induces its dimerization (Singh et al., 2015). Tyrosine phosphorylation in the absence of ligand was greatly decreased for the EphA2 Δjxtm-2 mutant (Figures 6A–6D). Treatment with saturating concentrations of the four dimeric ligands for 2.5 min, to capture the early effects of ligand-induced activation, increased tyrosine phosphorylation of EphA2 WT and the Δjxtm-1 mutant by several folds (Figures 6A–6D). Phosphorylation of EphA2 Δjxtm-2 was also in some cases slightly increased, but remained very low. These data suggest that the EphA2 juxtamembrane segment is important to enable appropriate arrangements of EphA2 intracellular regions for cross-phosphorylation on various tyrosine residues both in the absence and in the presence of ligands, regardless of the configuration of the ligand-binding domains.

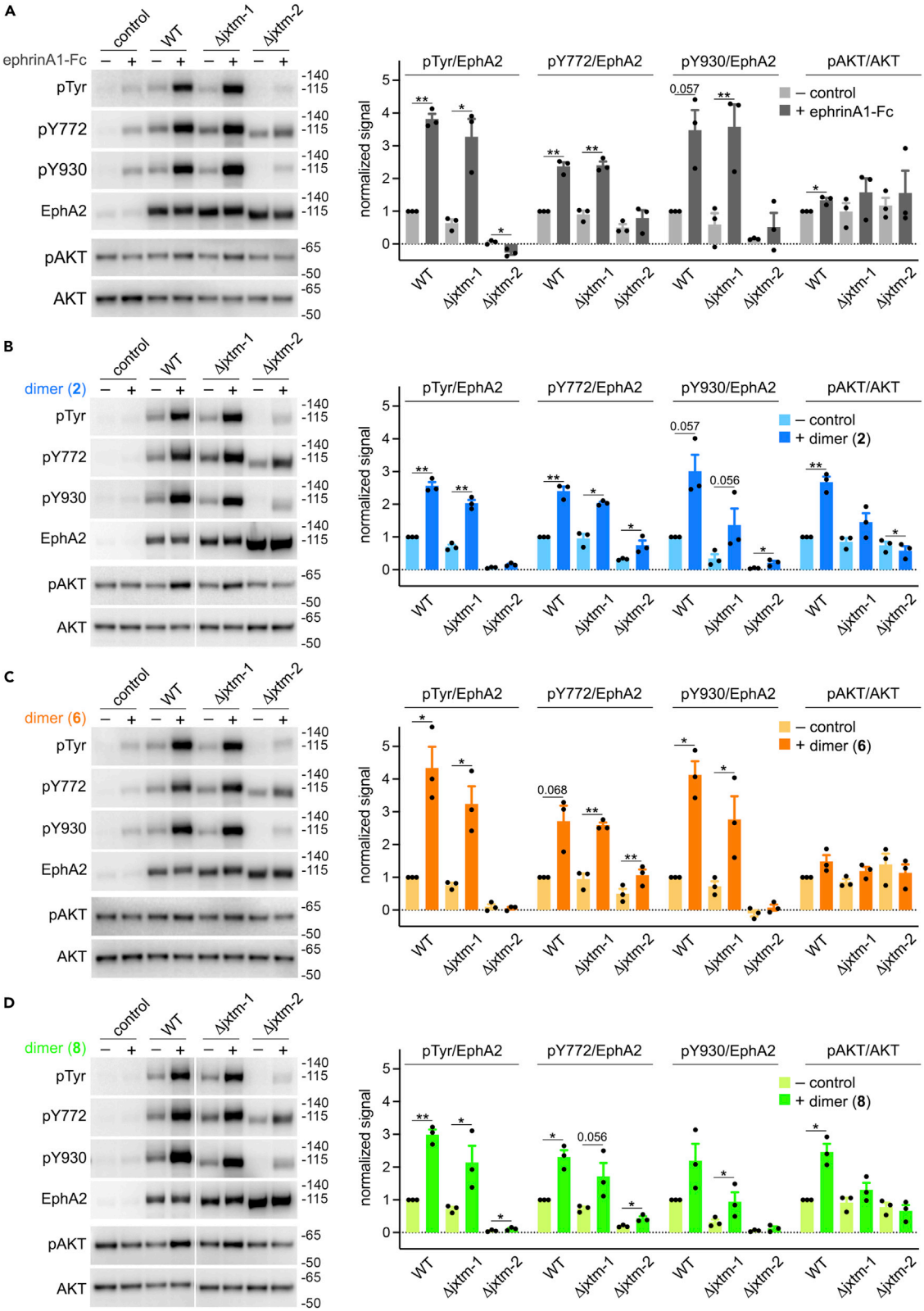
A
control
WT
Δjxtm-1
Δjxtm-2
ephrinA1-Fc
pTyr
pY772
pY930
EphA2
pAKT
AKT
pTyr/EphA2
pY772/EphA2
pY930/EphA2
pAKT/AKT
normalized signal
– control
+ ephrinA1-Fc
B
dimer (2)
– control
+ dimer (2)
C
dimer (6)
– control
+ dimer (6)
D
dimer (8)
– control
+ dimer (8)

Figure 6. The flexible juxtamembrane segment is required for EphA2 autophosphorylation

HEK293 cells stably transfected with EGFP as a control, EphA2 WT or the EphA2 juxtamembrane deletion mutantsΔQ565-L582 (Δjxtm-1) and ΔQ565-T606 (Δjxtm-2) were treated for 2.5 min with saturating concentrations of (A) ephrinA1-Fc, (B) dimer (**2**), (C) dimer (**6**) and (D) dimer (**8**). Lysates were probed by immunoblotting with the indicated antibodies. The vertical line in B and D indicates removal of irrelevant lanes. Molecular weight markers (in kDa) are indicated on the right. The graphs show quantifications normalized for each antibody to the cells expressing EphA2 WT and not treated with ligand (lighter bars). In the case of EphA2 phosphorylation, the background from control lanes (cells transfected with EGFP and not treated with ligand) was subtracted before normalizing to EphA2 levels. The error bars represent SEs and the individual measurements from 3 experiments are shown as dots. Statistical significance for the comparison between Δjxtm-1 or Δjxtm-2 cells treated with ligand and the corresponding untreated cells was determined by one-tailed paired t-test for EphA2 phosphorylation and two-tailed paired t-test for AKT phosphorylation. Statistical significance for the comparison between WT cells treated with ligand and untreated WT cells (which were used for normalization and thus set to a value of 1) was determined by one-sample t-test. *, $p < 0.05$ and **, $p < 0.01$; p values close to 0.05 are also shown. See also Figure S8.

We also assessed AKT S473 phosphorylation in the stably transfected HEK293 cells stimulated for 2.5 min with the four ligands. Unlike the AKT inhibition induced by EphA2 ligands in PC3 cells, in HEK293 cells expressing EphA2 WT we observed an increase in AKT phosphorylation. This discrepancy between PC3 cells and HEK293 cells is not surprising, given previous reports that EphA2 can activate AKT (Chang et al., 2008; Lim et al., 2019; Pasquale, 2010; Subbarayal et al., 2015) or inhibit AKT (Menges and McCance, 2008; Miao et al., 2015; Miao et al., 2009; Pasquale, 2010; Stallaert et al., 2018; Yang et al., 2011) in different cellular contexts. We found that peptide dimers (**2**) and (**8**) increase AKT phosphorylation more prominently than peptide (**6**) and ephrinA1-Fc (Figures 6A–6D). Furthermore, none of the ligands significantly affected AKT phosphorylation in cells expressing the EphA2 Δjxtm-1 and Δjxtm-2 mutants. Thus, both the EphA2 juxtamembrane segment and the type of arrangement of EphA2 molecules induced by dimers (**2**) and (**8**) appear to be important for strong AKT activation by EphA2. Treatment with the PI3-kinase inhibitor LY294002 shows that both basal and EphA2-induced AKT S473 phosphorylation in HEK293 cells depends on PI3-kinase activity (Figure S8), in agreement with previous findings that EphA2 can bind and activate PI3-kinase (Brantley-Sieders et al., 2004; Fang et al., 2008; Pandey et al., 1994). Interestingly, even though all four dimeric ligands can similarly activate EphA2 WT, the different effects on AKT phosphorylation of dimers (**2**) and (**8**) compared to dimer (**6**) and ephrinA1-Fc suggest differences in the signaling properties of EphA2 oligomers induced by the different ligands.

Distinct ligands differentially regulate EphA2 signaling

Consistent with the findings in HEK293 cells, in PC3 cells each peptide appears to have a unique profile of EphA2 pY588 phosphorylation and AKT inactivation (Figures 3A, 3D, and 3E), suggesting that the two responses can be differentially regulated by ligands. This observation that two EphA2 responses are differentially regulated by distinct ligands suggested that EphA2 may be capable of biased signaling. Ligand functional selectivity, or biased signaling, is a phenomenon that has been extensively studied for G protein-coupled receptors (GPCRs) but remains poorly documented for receptor tyrosine kinases (Karl et al., 2020; Kenakin and Christopoulos, 2013; Smith et al., 2018; Watson et al., 2014). We investigated the possibility of EphA2 biased signaling by analyzing the dose-response curves obtained with endogenous EphA2 in PC3 cells (Figure 3A), using approaches developed for GPCRs (Karl et al., 2020). This involves using EphA2 Y588 phosphorylation and AKT phosphorylation quantified at 15 min as a function of ligand concentration to determine and compare the potency (EC_{50}) and efficacy (E_{top}) for the two responses induced by different ligands (Rajagopal et al., 2011; Smith et al., 2018). We observed large differences among the ligands in the E_{top} values for Y588 phosphorylation (Figures 3C, 3D, and S9A), but not in the E_{top} values for AKT inhibition (Figures 3E and S9B). In terms of relative efficacies for pY588 versus pAKT inhibition, the C-terminally linked dimers and monomeric ligands behave differently from ephrinA1-Fc, while the N-terminally linked dimers and the head-to-tail dimer (**8**) are similar to ephrinA1-Fc (Figure S9C). Unlike the E_{top} values, when comparing the relative potency (EC_{50}) values for Y588 phosphorylation and inhibition of AKT phosphorylation, the N-terminally linked dimers and head-to-tail dimer (**8**) are all significantly different from ephrinA1-Fc (Figure S9D). Thus, the type of linkage affects EphA2 signaling properties induced by the dimeric peptides.

The determined EC_{50} and E_{top} values allowed us to calculate the bias factor β_{lig} for the two different responses induced by the various ligands relative to ephrinA1-Fc as the reference ligand (Rajagopal et al., 2011; Smith et al., 2018) (Figure S9E). This analysis suggests that all the peptides tested are biased ligands compared to ephrinA1-Fc and that they bias EphA2 signaling toward AKT inhibition relative to Y588 phosphorylation (Figures 1 and 7). Remarkably, the differential signaling originates from distinct mechanisms that depend on the class of ligands, with the N-terminally linked and head-to-tail dimers modulating

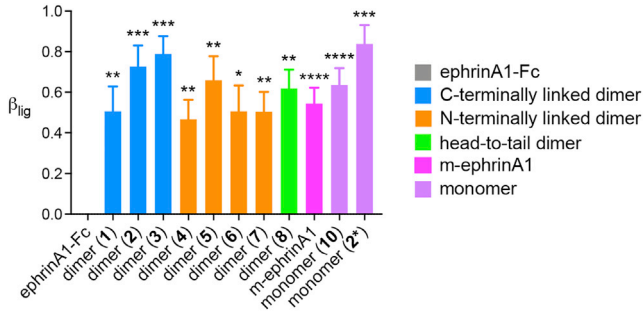

Figure 7. Evaluation of ligand bias in EphA2 signaling responses

The bias factor β_{lig} was calculated for the indicated ligands using ephrinA1-Fc as the reference ligand, as described in the Method Details section. The error bars represent SEs (calculated using propagation of errors) and the number of experiments is indicated in Figure 1. Statistical significance for the comparison of the different ligands with the reference ligand ephrinA1-Fc ($\beta_{lig} = 0$) was determined by one sample t test; *, $p < 0.05$; **, $p < 0.01$; ***, $p < 0.001$; ****, $p < 0.0001$. See also Figure S9.

relative potencies and the C-terminally-linked dimers and monomers modulating relative efficacies with respect to the reference ligand ephrinA1-Fc. Our findings support the notion that Eph receptors are capable of biased signaling and characterize a large set of rationally designed peptide ligands with diverse effects on the signaling profile of a receptor tyrosine kinase.

DISCUSSION

We have shown that very different arrangements of two LBDs in an EphA2 dimer are compatible with activation of receptor signaling. In our *in silico* models of a C-terminally linked or a head-to-tail dimeric peptide in complex with EphA2, the dimerization interface is engaged and the C-termini of the two EphA2 LBDs both face 'downwards'. This orientation is consistent with the orientation of the LBDs in the crystal structures of the EphA2 extracellular region (Himanen et al., 2010; Seiradake et al., 2010) and with the expected arrangement of full-length EphA2 dimers side-by-side on the cell surface (Figure S1). Indeed, measurements of EphA2 phosphorylation in cells show that the EphA2 dimeric configurations induced by C-terminally linked or head-to-tail dimeric peptides is well suited for EphA2 activation.

In our model of an N-terminally linked dimeric peptide in complex with EphA2, the C-termini of the two EphA2 LBDs have a different orientation. Extrapolating from crystal structures of the EphA2 extracellular region (such as PDB 3FL7) (Himanen et al., 2010), this orientation would place the membrane-proximal portions >230 Å apart from each other. This large distance should preclude cross-phosphorylation of dimeric EphA2 receptors bound to the N-terminally linked peptides. Unexpectedly, our immunoblotting data show that the N-terminally linked dimers are able to induce high maximal EphA2 autophosphorylation (E_{top} pY588) in PC3 cells. Thus, conformational changes in the EphA2 extracellular region and juxtamembrane segment might compensate for the altered orientation of the LBDs.

Our data with EphA2 juxtamembrane deletion mutants provide insights into signal propagation from the EphA2 extracellular region to the kinase domain. Whether the arrangement of the extracellular region can affect the arrangement of the intracellular region has been investigated for other families of receptor tyrosine kinases with contradictory results (Arkhipov et al., 2013; Bell et al., 2000; Doerner et al., 2015; Endres et al., 2013; Lu et al., 2010; Lu et al., 2012; Mi et al., 2011; Moriki et al., 2001; Sarabipour et al., 2016; Sarabipour and Hristova, 2016; Sorokin, 1995). We found that EphA2 lacking the entire juxtamembrane segment (Δjxtm-2 mutant) exhibits extremely low autophosphorylation. This suggests that in EphA2 WT the flexibility of the juxtamembrane segment decouples the extracellular and intracellular regions, enabling robust cross-phosphorylation in response to all ligands and even in the absence of ligand, regardless of the orientation of the LBDs. In addition, phosphorylation of different tyrosines presumably requires different arrangements of two EphA2 intracellular regions (functioning as "kinase" and "substrate"). This appears to depend on the juxtamembrane segment because we found that EphA2 autophosphorylation is almost completely lost in the absence of this flexible linker. Further investigation is needed to better understand the role of the juxtamembrane segment in EphA2 autophosphorylation and downstream signaling,

particularly in light of the fact that in some Eph receptors this linker can vary in length because of alternative splicing (Zisch and Pasquale, 1997), which may represent a mechanism to fine-tune signaling.

The higher potency of N-terminally linked and head-to-tail dimers compared with C-terminally linked dimers engineered from the same monomeric precursors may be due to interactions between the two EphA2 LBDs bound to the dimeric peptide. If the two LBDs bind independently, the K_d measured in ITC experiments for a dimeric peptide should be similar to that measured for the monomeric precursor and only the binding stoichiometry, N, should be different. However, the K_d measured for the N-terminally linked dimer (**5**) is 4-fold lower than for the corresponding monomer (**10**). This suggests positive cooperativity in the binding of the EphA2 LBDs to dimer (**5**), perhaps because of favorable interactions between them. In contrast, the K_d measured in ITC experiments for the C-terminally linked dimer (**2**) is 2-fold higher than for the corresponding monomers (**16***) and (**17***) (Gomez-Soler et al., 2019) (Table S2). This suggests negative cooperativity in the binding of the two EphA2 LBDs, perhaps because of steric hindrance or other unfavorable interactions between the bound LBDs. Thus, N-terminal dimerization appears to be associated with higher potency. In fact, dimers (**5**), (**6**) and (**7**), together with head-to-tail dimer (**8**), induce EphA2 activation even more potently than the dimeric ephrinA1-Fc and, to our knowledge, represent the most potent EphA2 agonists reported thus far.

Our fluorescence imaging data show that EphA2 dimers induced by both C-terminally linked peptide (**2**) and N-terminally linked peptide (**5**) form patches on the plasma membrane that likely contain large EphA2 oligomeric assemblies, an effect similar to that reported for ephrinA-Fc ligands (Salaita et al., 2010; Seiradake et al., 2013; Singh et al., 2018). Of note, our dimeric peptides induce EphA2 patches despite lacking the self-assembly promoting PhePhe sequence that has recently been proposed to be required for dimeric peptide-induced EphA2 aggregation in cells (Li et al., 2021). In these oligomers, the EphA2 kinase domains appear to be appropriately positioned for cross-phosphorylation within a dimer and/or possibly in trans between neighboring dimers, as previously described for the EGF receptor (Liang et al., 2018; Needham et al., 2016). Our FRET studies with EphA2 mutants that have impaired ability to assemble through a particular interface show that the C-terminally linked peptide (**2**) induces EphA2 oligomers that utilize both the dimerization and the clustering interfaces. In contrast, the N-terminally linked peptide (**5**) induces EphA2 oligomers that utilize the dimerization but not the clustering interface, in agreement with the predictions from our *in silico* modeling. Consistent with this, mutation of the clustering interface impairs EphA2 patching induced by C-terminally linked dimer (**2**) but not by N-terminally linked dimer (**5**). It is conceivable that these large oligomeric assemblies modulate EphA2 signaling responses, perhaps in a manner that depends on how the receptors interact with each other.

The availability of a collection of diverse ligands (including dimeric peptides with different configurations, monomeric peptides, m-ephrinA1 and ephrinA1-Fc) allowed us to uncover another intriguing aspect of EphA2 signaling, leading to the finding that EphA2 signaling responses can be differentially regulated by the activating ligand, likely through distinct mechanisms. We analyzed dose-response curves to identify and quantify bias. We compared two well known EphA2 signaling responses that can be reliably quantified for the endogenously expressed receptor, autophosphorylation on Y588 and downstream inhibition of AKT in PC3 prostate cancer cells stimulated with different ligands. A wide variety of responses have been used to determine biased signaling for GPCRs, including responses involving the receptor itself, such as receptor conformational changes measured with biosensors or receptor internalization (Kenakin and Christopoulos, 2013; Smith et al., 2018). Autophosphorylation on tyrosine residues is an early event in the ligand-induced activation of receptor tyrosine kinase downstream signaling networks and thus can provide direct evidence of biased signaling at the level of the receptor. We measured responses at 15 min, a time point when EphA2 Y588 phosphorylation and AKT dephosphorylation responses induced by all ligands are close to maximal and are not heavily influenced by the kinetics of EphA2 phosphorylation/dephosphorylation, EphA2 degradation, or recovery of AKT phosphorylation.

The calculated bias factor, β_{lig}, suggests that all of the peptides and m-ephrinA1 are significantly biased toward AKT inhibition when compared to ephrinA1-Fc. The factors responsible for the observed bias in EphA2 signaling responses are likely complex. The values of β_{lig} (which indicate the extent of the bias) do not seem to directly correlate with the configurations of the dimeric peptides (Figures 1 and 7). However, our data suggest that different classes of ligands can influence how bias is achieved. For example, the efficacy E_{top} (one of the factors contributing to bias) is lower for the Y588 phosphorylation response

induced by the C-terminally linked dimers and the monomers than by the other ligands (Figures 1, 3C, 3D, and S9A). Time courses with saturating ligand concentrations revealed that the peak pY588/EphA2 values occur at 5–10 min of stimulation and only slightly decrease by 15 min with all types of ligands examined. Thus, the C-terminally linked dimeric peptides and the monomeric peptides are partial agonists that cannot induce the highest levels of EphA2 Y588 phosphorylation (E_{top} pY588). In contrast, AKT phosphorylation is similarly inhibited to very low levels by all ligands, including the partial agonists (Figures 3E, 4D and S9B).

Previous evidence has suggested the possibility that the nature of the ligand may affect Eph receptor downstream signaling responses. For example, a peptide that binds to the EphA2 transmembrane helix has been shown to inhibit AKT signaling without affecting Y588 phosphorylation, and thus may represent an EphA2 biased agonist when compared to ephrinA1-Fc (Alves et al., 2018). In agreement with our findings, this study shows that EphA2 Y588 phosphorylation and AKT inhibition can be regulated differently by different EphA2 ligands. In addition, ephrinA1 immobilized on artificial lipid bilayers or nanocalipers can cause different EphA2 signaling responses depending on the size of the EphA2 oligomers induced (Verheyen et al., 2020; Xu et al., 2011). Finally, phosphoproteomics analyses have shown differences in the EphB2 signaling responses induced by the full-length transmembrane form of ephrinB1 compared to a truncated form lacking the intracellular portion (Jorgensen et al., 2009). It will be interesting to investigate in dose-response experiments whether ligand bias may be responsible for these signaling differences.

Another interesting observation emerging from the time-course experiments is that ephrinA1-Fc and monomeric peptide (**10**) induce more persistent AKT dephosphorylation than other ligands, with still very pronounced effects after 3 h of ligand stimulation. AKT dephosphorylation induced by EphA2 signaling in PC3 cells depends on a serine/threonine phosphatase (Yang et al., 2011). A similar decrease in AKT phosphorylation downstream of EphA2 has been observed in other cancer cell lines with high AKT phosphorylation, for example due to inactivation or loss of the lipid phosphatase PTEN or to growth factor stimulation (Boyd et al., 2014; Menges and McCance, 2008; Miao et al., 2015; Miao et al., 2009; Pasquale, 2010; Stallaert et al., 2018; Yang et al., 2011). In contrast, EphA2 may preferentially activate the PI3 kinase-AKT axis in cells (such as non-transformed cells) where AKT activity is low (Boyd et al., 2014; Brantley-Sieders et al., 2004; Chang et al., 2008; Lim et al., 2019; Pandey et al., 1994; Pasquale, 2010; Subbarayal et al., 2015). Indeed, in non-transformed HEK293 cells stably overexpressing EphA2, we observed an increase in AKT phosphorylation, particularly in response to C-terminally linked dimer (**2**) and head-to-tail dimer (**8**). Dose-response studies are needed to determine whether these differences are a consequence of EphA2 biased signaling in HEK293 cells. AKT activation downstream of EphA2 appears to require the juxtamembrane segment and, as also previously shown by others, PI3 kinase activation (Pandey et al., 1994). Further work will also be needed to characterize the mechanism underlying the differential regulation of PI3 kinase by different ligands and whether it might involve differential phosphorylation of Y735 in the EphA2 kinase domain, which is a known binding site for the SH2 domain of the PI3 kinase p85 regulatory subunit of PI3 kinase (Fang et al., 2008).

In conclusion, we have engineered different classes of peptide ligands able to stimulate EphA2 signaling responses with unprecedented subnanomolar potency and high selectivity. While this work was in progress, several other dimeric YSA derivative peptides have been reported, which appear to be less potent and have generally been used to stimulate cells at micromolar concentrations (Gambini et al., 2018; Li et al., 2021; Salem et al., 2020a; Salem et al., 2020b; Salem et al., 2018). Developing different classes of peptide ligands enabled us to demonstrate that ligands can differentially regulate EphA2 signaling through different mechanisms. Our findings imply that ligands can be engineered to favor desired Eph receptor signaling responses and functional outcomes. This suggests that biased ligands could be tailored to modulate Eph receptor signaling as needed to treat a particular disease, potentially favoring beneficial effects over unwanted side-effects. For example, against cancer it would be desirable to develop ligands biased toward inhibition of major oncogenic pathways, such as AKT-mTORC1 and RAS-ERK (Miao et al., 2001; Yang et al., 2011). Alternatively, ligands biased toward promoting EphA2 endocytosis could be useful for delivery of conjugated drugs into EphA2-expressing cells (Guo et al., 2015; Mudd et al., 2020; Salem et al., 2018; Wang et al., 2012) or for removal of EphA2 from the cell surface to inhibit certain parasitic infections (Barquilla and Pasquale, 2015; Gomez-Soler and Pasquale, 2021). Finally, ligands that favor EphA2 degradation could be used to inhibit the oncogenic effects of EphA2 non-canonical signaling through S897 phosphorylation (Barquilla and Pasquale, 2015; Miao et al., 2009; Wilson et al., 2021). Such ligands may offer

an alternative to the more challenging proteolysis-targeting chimera (PROTAC) and similar technologies (Burslem et al., 2018; Donovan et al., 2020). Better understanding of the mechanisms underlying EphA2 biased signaling will enable the design of ligands that can fine-tune the nature and persistence of EphA2 signaling responses as needed.

Limitations of the study

Given the laborious nature of the experiments and the need for sensitive and accurate methods to monitor signaling responses, our studies are limited to providing proof-of-principle for EphA2 biased signaling through examination of two signaling responses: EphA2 autophosphorylation on Y588 and inhibition of AKT phosphorylation on S473. Bias in other EphA2 autophosphorylation sites and downstream signaling responses merits further investigation. It could also be informative to examine EphA2 signaling bias in additional cellular contexts and the effects of signaling kinetics on bias by measuring bias at different times after ligand stimulation. It will also be interesting to explore the mechanisms responsible for the differential effects of distinct ligands on EphA2 signaling responses, including the importance of different EphA2 conformations and oligomeric arrangements and the mechanism underlying the efficacy of EphA2 autophosphorylation and AKT inhibition. Additional studies are also needed to investigate biased signaling by other Eph receptors. Finally, the factors that differentially regulate the rate of EphA2 degradation in response to different ligands also remain to be determined.

STAR★METHODS

Detailed methods are provided in the online version of this paper and include the following:

- KEY RESOURCES TABLE
- RESOURCE AVAILABILITY
  - Lead contact
  - Materials availability
  - Data and code availability
- METHOD DETAILS
  - Peptide synthesis and design
  - *In silico* modeling
  - Isothermal titration calorimetry (ITC)
  - ELISAs
  - EphA2 constructs
  - Immunoblotting
  - Cell retraction
  - Analysis of ligand bias
  - Förster resonance energy transfer (FRET)
- QUANTIFICATION AND STATISTICAL ANALYSIS

SUPPLEMENTAL INFORMATION

Supplemental information can be found online at https://doi.org/10.1016/j.isci.2022.103870

ACKNOWLEDGMENTS

The authors thank Andrey Bobkov (SBP Protein Analysis Core) for performing ITC experiments and Małgorzata Dobaczewska for help with protein expression and purification. This work was supported by NIH grants R01GM131374 (to EBP and KH), institutional funding (to EBP) and NCI Cancer Center Support Grant P30CA030199, which funded SBP Core Facilities. The content is solely the responsibility of the authors and does not necessarily represent the official views of the NIH.

AUTHOR CONTRIBUTIONS

MGS: investigation, validation, writing – review and editing: MPG: investigation; BCL: conceptualization, investigation, writing – original draft preparation, writing – review and editing, visualization; EZM: investigation, formal analysis, writing – review and editing, visualization; AR, investigation; MWM, investigation; KH, conceptualization, methodology, validation, writing – review and editing, supervision, project administration, funding acquisition; EBP, conceptualization, investigation, methodology, validation, formal

analysis, writing – original draft preparation, writing – review and editing, visualization, supervision, project administration, funding acquisition.

DECLARATION OF INTERESTS

BCL and EBP are inventors on a filed provisional patent application on the EphA2-targeting peptides. All other authors declare no competing interests.

Received: September 8, 2021
Revised: December 13, 2021
Accepted: February 1, 2022
Published: March 18, 2022

REFERENCES

Alves, D.S., Westerfield, J.M., Shi, X., Nguyen, V.P., Stefanski, K.M., Booth, K.R., Kim, S., Morrell-Falvey, J., Wang, B.C., Abel, S.M., et al. (2018). A novel pH-dependent membrane peptide that binds to EphA2 and inhibits cell migration. Elife *7*. https://doi.org/10.7554/eLife.36645.

Arkhipov, A., Shan, Y., Das, R., Endres, N.F., Eastwood, M.P., Wemmer, D.E., Kuriyan, J., and Shaw, D.E. (2013). Architecture and membrane interactions of the EGF receptor. Cell *152*, 557–569. https://doi.org/10.1016/j.cell.2012.12.030.

Barquilla, A., Lamberto, I., Noberini, R., Heynen-Genel, S., Brill, L.M., and Pasquale, E.B. (2016). Protein kinase A can block EphA2 receptor-mediated cell repulsion by increasing EphA2 S897 phosphorylation. Mol. Biol. Cell *27*, 2757–2770. https://doi.org/10.1091/mbc.E16-01-0048.

Barquilla, A., and Pasquale, E.B. (2015). Eph receptors and ephrins: therapeutic opportunities. Annu. Rev. Pharmacol.Toxicol. *55*, 465–487. https://doi.org/10.1146/annurev-pharmtox-011112-140226.

Beauchamp, A., Lively, M.O., Mintz, A., Gibo, D., Wykosky, J., and Debinski, W. (2012). EphrinA1 is released in three forms from cancer cells by matrix metalloproteases. Mol. Cell Biol. *32*, 3253–3264. https://doi.org/10.1128/MCB.06791-11.

Bell, C.A., Tynan, J.A., Hart, K.C., Meyer, A.N., Robertson, S.C., and Donoghue, D.J. (2000). Rotational coupling of the transmembrane and kinase domains of the Neu receptor tyrosine kinase. Mol. Biol. Cell *11*, 3589–3599. https://doi.org/10.1091/mbc.11.10.3589.

Biao-Xue, R., Xi-Guang, C., Shuan-Ying, Y., Wei, L., and Zong-Juan, M. (2011). EphA2-dependent molecular targeting therapy for malignant tumors. Curr. Cancer Drug Targets *11*, 1082–1097. https://doi.org/10.2174/156800911798073050.

Boyd, A.W., Bartlett, P.F., and Lackmann, M. (2014). Therapeutic targeting of EPH receptors and their ligands. Nat. Rev. Drug Discov. *13*, 39–62. https://doi.org/10.1038/nrd4175.

Brantley-Sieders, D.M., Caughron, J., Hicks, D., Pozzi, A., Ruiz, J.C., and Chen, J. (2004). EphA2 receptor tyrosine kinase regulates endothelial cell migration and vascular assembly through phosphoinositide 3-kinase-mediated Rac1 GTPase activation. J. Cell Sci. *117*, 2037–2049. https://doi.org/10.1242/jcs.01061.

Burslem, G.M., Smith, B.E., Lai, A.C., Jaime-Figueroa, S., McQuaid, D.C., Bondeson, D.P., Toure, M., Dong, H., Qian, Y., Wang, J., et al. (2018). The advantages of targeted protein degradation over inhibition: an RTK case study. Cell Chem Biol. *25*, 67–77.e63. https://doi.org/10.1016/j.chembiol.2017.09.009.

Chang, Q., Jorgensen, C., Pawson, T., and Hedley, D.W. (2008). Effects of dasatinib on EphA2 receptor tyrosine kinase activity and downstream signalling in pancreatic cancer. Br. J. Cancer *99*, 1074–1082. https://doi.org/10.1038/sj.bjc.6604676.

Cheng, C., Ansari, M.M., Cooper, J.A., and Gong, X. (2013). EphA2 and Src regulate equatorial cell morphogenesis during lens development. Development *140*, 4237–4245. https://doi.org/10.1242/dev.100727.

Cheng, N., Brantley, D.M., Liu, H., Lin, Q., Enriquez, M., Gale, N., Yancopoulos, G., Cerretti, D.P., Daniel, T.O., and Chen, J. (2002). Blockade of EphA receptor tyrosine kinase activation inhibits vascular endothelial cell growth factor-induced angiogenesis. Mol. Cancer Res. *1*, 2–11.

Copeland, R.A., Pompliano, D.L., and Meek, T.D. (2006). Drug-target residence time and its implications for lead optimization. Nat. Rev. Drug Discov. *5*, 730–739. https://doi.org/10.1038/nrd2082.

Coulthard, M.G., Morgan, M., Woodruff, T.M., Arumugam, T.V., Taylor, S.M., Carpenter, T.C., Lackmann, M., and Boyd, A.W. (2012). Eph/Ephrin signaling in injury and inflammation. Am. J. Pathol. *181*, 1493–1503. https://doi.org/10.1016/j.ajpath.2012.06.043.

Cullen, B.R. (2000). Utility of the secreted placental alkaline phosphatase reporter enzyme. Methods Enzymol. *326*, 159–164. https://doi.org/10.1016/s0076-6879(00)26053-9.

Doerner, A., Scheck, R., and Schepartz, A. (2015). Growth factor identity is encoded by discrete coiled-coil rotamers in the EGFR juxtamembrane region. Chem. Biol. *22*, 776–784. https://doi.org/10.1016/j.chembiol.2015.05.008.

Donovan, K.A., Ferguson, F.M., Bushman, J.W., Eleuteri, N.A., Bhunia, D., Ryu, S., Tan, L., Shi, K., Yue, H., Liu, X., et al. (2020). Mapping the degradable kinome provides a resource for expedited degrader development. Cell *183*, 1714–1731.e1710. https://doi.org/10.1016/j.cell.2020.10.038.

Duggineni, S., Mitra, S., Lamberto, I., Han, X., Xu, Y., An, J., Pasquale, E.B., and Huang, Z. (2013). Design and synthesis of potent bivalent peptide agonists targeting the EphA2 receptor. ACS Med. Chem. Lett. *4*, 344–348. https://doi.org/10.1021/ml3004523.

Endres, N.F., Das, R., Smith, A.W., Arkhipov, A., Kovacs, E., Huang, Y., Pelton, J.G., Shan, Y., Shaw, D.E., Wemmer, D.E., et al. (2013). Conformational coupling across the plasma membrane in activation of the EGF receptor. Cell *152*, 543–556. https://doi.org/10.1016/j.cell.2012.12.032.

Fang, W.B., Brantley-Sieders, D.M., Hwang, Y., Ham, A.J., and Chen, J. (2008). Identification and functional analysis of phosphorylated tyrosine residues within EphA2 receptor tyrosine kinase. J. Biol. Chem. *283*, 16017–16026. https://doi.org/10.1074/jbc.M709934200.

Finney, A.C., Funk, S.D., Green, J.M., Yurdagul, A., Jr., Rana, M.A., Pistorius, R., Henry, M., Yurochko, A., Pattillo, C.B., Traylor, J.G., et al. (2017). EphA2 expression regulates inflammation and fibroproliferative remodeling in atherosclerosis. Circulation *136*, 566–582. https://doi.org/10.1161/CIRCULATIONAHA.116.026644.

Flanagan, J.G., Cheng, H.J., Feldheim, D.A., Hattori, M., Lu, Q., and Vanderhaeghen, P. (2000). Alkaline phosphatase fusions of ligands or receptors as in situ probes for staining of cells, tissues, and embryos. Methods Enzymol. *327*, 19–35. https://doi.org/10.1016/s0076-6879(00)27264-9.

Funk, S.D., and Orr, A.W. (2013). Ephs and ephrins resurface in inflammation, immunity, and atherosclerosis. Pharmacol. Res. *67*, 42–52. https://doi.org/10.1016/j.phrs.2012.10.008.

Gambini, L., Salem, A.F., Udompholkul, P., Tan, X.F., Baggio, C., Shah, N., Aronson, A., Song, J., and Pellecchia, M. (2018). Structure-based design of novel EphA2 agonistic agents with nanomolar affinity in vitro and in cell. ACS Chem. Biol. *13*, 2633–2644. https://doi.org/10.1021/acschembio.8b00556.

Gomez-Soler, M., and Pasquale, E.B. (2021). Eph receptors and ephrins. In Encyclopedia of Molecular Pharmacology, S. Offermanns and W. Rosenthal, eds. (Springer Nature), pp. 615–628, in press. https://doi.org/10.1007/978-3-030-21573-6_10045-1.

Gomez-Soler, M., Petersen Gehring, M., Lechtenberg, B.C., Zapata-Mercado, E., Hristova, K., and Pasquale, E.B. (2019). Engineering nanomolar peptide ligands that differentially modulate EphA2 receptor signaling. J. Biol. Chem. *294*, 8791–8805. https://doi.org/10.1074/jbc.RA119.008213.

Gordon, K., Kochkodan, J.J., Blatt, H., Lin, S.Y., Kaplan, N., Johnston, A., Swindell, W.R., Hoover, P., Schlosser, B.J., Elder, J.T., et al. (2013). Alteration of the EphA2/Ephrin-A signaling axis in psoriatic epidermis. J.Invest Dermatol. *133*, 712–722. https://doi.org/10.1038/jid.2012.391.

Guo, Z., He, B., Yuan, L., Dai, W., Zhang, H., Wang, X., Wang, J., Zhang, X., and Zhang, Q. (2015). Dual targeting for metastatic breast cancer and tumor neovasculature by EphA2-mediated nanocarriers. Int. J. Pharm. *493*, 380–389. https://doi.org/10.1016/j.ijpharm.2015.05.051.

Harada, K., Negishi, M., and Katoh, H. (2015). HGF-induced serine 897 phosphorylation of EphA2 regulates epithelial morphogenesis of MDCK cells in 3D culture. J.Cell Sci *128*, 1912–1921. https://doi.org/10.1242/jcs.163790.

Himanen, J.P., Yermekbayeva, L., Janes, P.W., Walker, J.R., Xu, K., Atapattu, L., Rajashankar, K.R., Mensinga, A., Lackmann, M., Nikolov, D.B., and Dhe-Paganon, S. (2010). Architecture of Eph receptor clusters. Proc. Natl. Acad. Sci. U S A *107*, 10860–10865. https://doi.org/10.1073/pnas.1004148107.

Jorgensen, C., Sherman, A., Chen, G.I., Pasculescu, A., Poliakov, A., Hsiung, M., Larsen, B., Wilkinson, D.G., Linding, R., and Pawson, T. (2009). Cell-specific information processing in segregating populations of Eph receptor ephrin-expressing cells. Science *326*, 1502–1509. https://doi.org/10.1126/science.1176615.

Karl, K., Paul, M.D., Pasquale, E.B., and Hristova, K. (2020). Ligand bias in receptor tyrosine kinase signaling. J. Biol. Chem. *295*, 18494–18507. https://doi.org/10.1074/jbc.REV120.015190.

Kenakin, T. (2019). Biased receptor signaling in drug discovery. Pharmacol. Rev. *71*, 267–315. https://doi.org/10.1124/pr.118.016790.

Kenakin, T., and Christopoulos, A. (2013). Signalling bias in new drug discovery: detection, quantification and therapeutic impact. Nat. Rev. Drug Discov. *12*, 205–216. https://doi.org/10.1038/nrd3954.

King, C., Raicu, V., and Hristova, K. (2017). Understanding the FRET signatures of interacting membrane proteins. J. Biol. Chem. *292*, 5291–5310. https://doi.org/10.1074/jbc.M116.764282.

King, C., Stoneman, M., Raicu, V., and Hristova, K. (2016). Fully quantified spectral imaging reveals in vivo membrane protein interactions. Integr. Biol. (Camb) *8*, 216–229. https://doi.org/10.1039/c5ib00202h.

Koolpe, M., Dail, M., and Pasquale, E.B. (2002). An ephrin mimetic peptide that selectively targets the EphA2 receptor. J. Biol. Chem. *277*, 46974–46979. https://doi.org/10.1074/jbc.M208495200.

Kozakov, D., Hall, D.R., Xia, B., Porter, K.A., Padhorny, D., Yueh, C., Beglov, D., and Vajda, S. (2017). The ClusPro web server for protein-protein docking. Nat. Protoc. *12*, 255–278. https://doi.org/10.1038/nprot.2016.169.

Lamberto, I., Lechtenberg, B.C., Olson, E.J., Mace, P.D., Dawson, P.E., Riedl, S.J., and Pasquale, E.B. (2014). Development and structural analysis of a nanomolar cyclic peptide antagonist for the EphA4 receptor. ACS Chem. Biol. *9*, 2787–2795. https://doi.org/10.1021/cb500677x.

Li, J., Fang, Y., Zhang, Y., Wang, H., Yang, Z., and Ding, D. (2021). Supramolecular self-assembly-facilitated aggregation of tumor-specific transmembrane receptors for signaling activation and converting immunologically cold to hot tumors. Adv. Mater. *33*, e2008518. https://doi.org/10.1002/adma.202008518.

Liang, S.I., van Lengerich, B., Eichel, K., Cha, M., Patterson, D.M., Yoon, T.Y., von Zastrow, M., Jura, N., and Gartner, Z.J. (2018). Phosphorylated EGFR dimers are not sufficient to activate ras. Cell Rep. *22*, 2593–2600. https://doi.org/10.1016/j.celrep.2018.02.031.

Light, T.P., Brun, D., Guardado-Calvo, P., Pederzoli, R., Haouz, A., Neipel, F., Rey, F.A., Hristova, K., and Backovic, M. (2021). Human herpesvirus 8 molecular mimicry of ephrin ligands facilitates cell entry and triggers EphA2 signaling. Plos Biol. *19*, e3001392. https://doi.org/10.1371/journal.pbio.3001392.

Lim, W., Bae, H., Bazer, F.W., and Song, G. (2019). Ephrin A1 promotes proliferation of bovine endometrial cells with abundant expression of proliferating cell nuclear antigen and cyclin D1 changing the cell population at each stage of the cell cycle. J. Cell Physiol. *234*, 4864–4873. https://doi.org/10.1002/jcp.27275.

Lin, S., Gordon, K., Kaplan, N., and Getsios, S. (2010). Ligand targeting of EphA2 enhances keratinocyte adhesion and differentiation via desmoglein 1. Mol. Biol. Cell *21*, 3902–3914. https://doi.org/10.1091/mbc.E10-03-0242.

Lodola, A., Giorgio, C., Incerti, M., Zanotti, I., and Tognolini, M. (2017). Targeting Eph/ephrin system in cancer therapy. Eur. J. Med. Chem. *142*, 152–162. https://doi.org/10.1016/j.ejmech.2017.07.029.

London, N., Raveh, B., Cohen, E., Fathi, G., and Schueler-Furman, O. (2011). Rosetta FlexPepDock web server–high resolution modeling of peptide-protein interactions. Nucleic Acids Res. *39*, W249–W253. https://doi.org/10.1093/nar/gkr431.

Lu, C., Mi, L.Z., Grey, M.J., Zhu, J., Graef, E., Yokoyama, S., and Springer, T.A. (2010). Structural evidence for loose linkage between ligand binding and kinase activation in the epidermal growth factor receptor. Mol. Cell Biol. *30*, 5432–5443. https://doi.org/10.1128/MCB.00742-10.

Lu, C., Mi, L.Z., Schurpf, T., Walz, T., and Springer, T.A. (2012). Mechanisms for kinase-mediated dimerization of the epidermal growth factor receptor. J. Biol. Chem. *287*, 38244–38253. https://doi.org/10.1074/jbc.M112.414391.

Menges, C.W., and McCance, D.J. (2008). Constitutive activation of the Raf-MAPK pathway causes negative feedback inhibition of Ras-PI3K-AKT and cellular arrest through the EphA2 receptor. Oncogene *27*, 2934–2940. https://doi.org/10.1038/sj.onc.1210957.

Mi, L.Z., Lu, C., Li, Z., Nishida, N., Walz, T., and Springer, T.A. (2011). Simultaneous visualization of the extracellular and cytoplasmic domains of the epidermal growth factor receptor. Nat. Struct. Mol. Biol. *18*, 984–989. https://doi.org/10.1038/nsmb.2092.

Miao, H., Gale, N.W., Guo, H., Qian, J., Petty, A., Kaspar, J., Murphy, A.J., Valenzuela, D.M., Yancopoulos, G., Hambardzumyan, D., et al. (2015). EphA2 promotes infiltrative invasion of glioma stem cells in vivo through cross-talk with Akt and regulates stem cell properties. Oncogene *34*, 558–567. https://doi.org/10.1038/onc.2013.590.

Miao, H., Li, D.Q., Mukherjee, A., Guo, H., Petty, A., Cutter, J., Basilion, J.P., Sedor, J., Wu, J., Danielpour, D., et al. (2009). EphA2 mediates ligand-dependent inhibition and ligand-independent promotion of cell migration and invasion via a reciprocal regulatory loop with Akt. Cancer Cell *16*, 9–20. https://doi.org/10.1016/j.ccr.2009.04.009.

Miao, H., Wei, B.R., Peehl, D.M., Li, Q., Alexandrou, T., Schelling, J.R., Rhim, J.S., Sedor, J.R., Burnett, E., and Wang, B.C. (2001). Activation of EphA receptor tyrosine kinase inhibits the Ras/MAPK pathway. Nat. Cell Biol. *3*, 527–530. https://doi.org/10.1038/35074604.

Miura, K., Nam, J.M., Kojima, C., Mochizuki, N., and Sabe, H. (2009). EphA2 engages Git1 to suppress Arf6 activity modulating epithelial cell-cell contacts. Mol. Biol. Cell *20*, 1949–1959. https://doi.org/10.1091/mbc.E08-06-0549.

Moriki, T., Maruyama, H., and Maruyama, I.N. (2001). Activation of preformed EGF receptor dimers by ligand-induced rotation of the transmembrane domain. J. Mol. Biol. *311*, 1011–1026. https://doi.org/10.1006/jmbi.2001.4923.

Mudd, G.E., Brown, A., Chen, L., van Rietschoten, K., Watcham, S., Teufel, D.P., Pavan, S., Lani, R., Huxley, P., and Bennett, G.S. (2020). Identification and optimization of EphA2-selective bicycles for the delivery of cytotoxic payloads. J. Med. Chem. *63*, 4107–4116. https://doi.org/10.1021/acs.jmedchem.9b02129.

Needham, S.R., Roberts, S.K., Arkhipov, A., Mysore, V.P., Tynan, C.J., Zanetti-Domingues, L.C., Kim, E.T., Losasso, V., Korovesis, D., Hirsch, M., et al. (2016). EGFR oligomerization organizes kinase-active dimers into competent signalling platforms. Nat. Commun. *7*, 13307. https://doi.org/10.1038/ncomms13307.

Noberini, R., Rubio de la Torre, E., and Pasquale, E.B. (2012). Profiling Eph receptor expression in cells and tissues: a targeted mass spectrometry approach. Cell Adh Migr *6*, 102–112. https://doi.org/10.4161/cam.19620.

Ogawa, K., Pasqualini, R., Lindberg, R.A., Kain, R., Freeman, A.L., and Pasquale, E.B. (2000). The ephrin-A1 ligand and its receptor, EphA2, are expressed during tumor neovascularization. Oncogene *19*, 6043–6052. https://doi.org/10.1038/sj.onc.1204004.

Onaran, H.O., Ambrosio, C., Ugur, O., Madaras Koncz, E., Gro, M.C., Vezzi, V., Rajagopal, S., and Costa, T. (2017). Systematic errors in detecting

biased agonism: analysis of current methods and development of a new model-free approach. Sci. Rep. *7*, 44247. https://doi.org/10.1038/srep44247.

Pandey, A., Lazar, D.F., Saltiel, A.R., and Dixit, V.M. (1994). Activation of the Eck receptor protein tyrosine kinase stimulates phosphatidylinositol 3-kinase activity. J. Biol. Chem. *269*, 30154–30157.

Pandey, A., Shao, H., Marks, R.M., Polverini, P.J., and Dixit, V.M. (1995). Role of B61, the ligand for the Eck receptor tyrosine kinase, in TNF-alpha-induced angiogenesis. Science *268*, 567–569. https://doi.org/10.1126/science.7536959.

Park, J.E., Son, A.I., Hua, R., Wang, L., Zhang, X., and Zhou, R. (2012). Human cataract mutations in EPHA2 SAM domain alter receptor stability and function. PLoS One *7*, e36564. https://doi.org/10.1371/journal.pone.0036564.

Pasquale, E.B. (2005). Eph receptor signalling casts a wide net on cell behaviour. Nat. Rev. Mol. Cell Biol. *6*, 462–475. https://doi.org/10.1038/nrm1662.

Pasquale, E.B. (2010). Eph receptors and ephrins in cancer: bidirectional signalling and beyond. Nat. Rev. Cancer *10*, 165–180. https://doi.org/10.1038/nrc2806.

Porazinski, S., de Navascues, J., Yako, Y., Hill, W., Jones, M.R., Maddison, R., Fujita, Y., and Hogan, C. (2016). EphA2 drives the segregation of ras-transformed epithelial cells from normal neighbors. Curr. Biol. *26*, 3220–3229. https://doi.org/10.1016/j.cub.2016.09.037.

Rajagopal, S., Ahn, S., Rominger, D.H., Gowen-MacDonald, W., Lam, C.M., Dewire, S.M., Violin, J.D., and Lefkowitz, R.J. (2011). Quantifying ligand bias at seven-transmembrane receptors. Mol. Pharmacol. *80*, 367–377. https://doi.org/10.1124/mol.111.072801.

Ramirez-Aportela, E., Lopez-Blanco, J.R., and Chacon, P. (2016). Frodock 2.0: fast protein-protein docking server. Bioinformatics *32*, 2386–2388. https://doi.org/10.1093/bioinformatics/btw141.

Riedl, S.J., and Pasquale, E.B. (2015). Targeting the Eph system with peptides and peptide conjugates. Curr. Drug Targets *16*, 1031–1047. https://doi.org/10.2174/1389450116666150727115934.

Salaita, K., Nair, P.M., Petit, R.S., Neve, R.M., Das, D., Gray, J.W., and Groves, J.T. (2010). Restriction of receptor movement alters cellular response: physical force sensing by EphA2. Science *327*, 1380–1385. https://doi.org/10.1126/science.1181729.

Salem, A.F., Gambini, L., Billet, S., Sun, Y., Oshiro, H., Zhao, M., Hoffman, R.M., Bhowmick, N.A., and Pellecchia, M. (2020a). Prostate cancer metastases are strongly inhibited by agonistic Epha2 ligands in an orthotopic mouse model. Cancers (Basel) *12*. https://doi.org/10.3390/cancers12102854.

Salem, A.F., Gambini, L., Udompholkul, P., Baggio, C., and Pellecchia, M. (2020b). Therapeutic targeting of pancreatic cancer via EphA2 dimeric agonistic agents. Pharmaceuticals (Basel) *13*. https://doi.org/10.3390/ph13050090.

Salem, A.F., Wang, S., Billet, S., Chen, J.F., Udompholkul, P., Gambini, L., Baggio, C., Tseng, H.R., Posadas, E.M., Bhowmick, N.A., and Pellecchia, M. (2018). Reduction of circulating cancer cells and metastases in breast-cancer models by a potent EphA2-agonistic peptide-drug conjugate. J. Med. Chem. *61*, 2052–2061. https://doi.org/10.1021/acs.jmedchem.7b01837.

Sarabipour, S., Ballmer-Hofer, K., and Hristova, K. (2016). VEGFR-2 conformational switch in response to ligand binding. Elife *5*, e13876. https://doi.org/10.7554/eLife.13876.

Sarabipour, S., and Hristova, K. (2016). Mechanism of FGF receptor dimerization and activation. Nat. Commun. *7*, 10262. https://doi.org/10.1038/ncomms10262.

Schuetz, D.A., de Witte, W.E.A., Wong, Y.C., Knasmueller, B., Richter, L., Kokh, D.B., Sadiq, S.K., Bosma, R., Nederpelt, I., Heitman, L.H., et al. (2017). Kinetics for Drug Discovery: an industry-driven effort to target drug residence time. Drug Discov. Today *22*, 896–911. https://doi.org/10.1016/j.drudis.2017.02.002.

Seiradake, E., Harlos, K., Sutton, G., Aricescu, A.R., and Jones, E.Y. (2010). An extracellular steric seeding mechanism for Eph-ephrin signaling platform assembly. Nat. Struct. Mol. Biol. *17*, 398–402. https://doi.org/10.1038/nsmb.1782.

Seiradake, E., Schaupp, A., del Toro Ruiz, D., Kaufmann, R., Mitakidis, N., Harlos, K., Aricescu, A.R., Klein, R., and Jones, E.Y. (2013). Structurally encoded intraclass differences in EphA clusters drive distinct cell responses. Nat. Struct. Mol. Biol. *20*, 958–964. https://doi.org/10.1038/nsmb.2617.

Shiels, A., Bennett, T.M., Knopf, H.L., Maraini, G., Li, A., Jiao, X., and Hejtmancik, J.F. (2008). The EPHA2 gene is associated with cataracts linked to chromosome 1p. Mol. Vis. *14*, 2042–2055.

Singh, D.R., Ahmed, F., King, C., Gupta, N., Salotto, M., Pasquale, E.B., and Hristova, K. (2015). EphA2 receptor unliganded dimers suppress EphA2 pro-tumorigenic signaling. J. Biol. Chem. *290*, 27271–27279. https://doi.org/10.1074/jbc.M115.676866.

Singh, D.R., Ahmed, F., Paul, M.D., Gedam, M., Pasquale, E.B., and Hristova, K. (2017a). The SAM domain inhibits EphA2 interactions in the plasma membrane. Biochim. Biophys. Acta *1864*, 31–38. https://doi.org/10.1016/j.bbamcr.2016.10.011.

Singh, D.R., Ahmed, F., Sarabipour, S., and Hristova, K. (2017b). Intracellular domain contacts contribute to Ecadherin constitutive dimerization in the plasma membrane. J. Mol. Biol. *429*, 2231–2245. https://doi.org/10.1016/j.jmb.2017.05.020.

Singh, D.R., Kanvinde, P., King, C., Pasquale, E.B., and Hristova, K. (2018). The EphA2 receptor is activated through induction of distinct, ligand-dependent oligomeric structures. Commun. Biol. *1*, 15. https://doi.org/10.1038/s42003-018-0017-7.

Singh, D.R., Pasquale, E.B., and Hristova, K. (2016). A small peptide promotes EphA2 kinase-dependent signaling by stabilizing EphA2 dimers. Biochim. Biophys. Acta *1860*, 1922–1928. https://doi.org/10.1016/j.bbagen.2016.06.004.

Smith, J.S., Lefkowitz, R.J., and Rajagopal, S. (2018). Biased signalling: from simple switches to allosteric microprocessors. Nat. Rev. Drug Discov. *17*, 243–260. https://doi.org/10.1038/nrd.2017.229.

Sorokin, A. (1995). Activation of the EGF receptor by insertional mutations in its juxtamembrane regions. Oncogene *11*, 1531–1540.

Stallaert, W., Bruggemann, Y., Sabet, O., Baak, L., Gattiglio, M., and Bastiaens, P.I.H. (2018). Contact inhibitory Eph signaling suppresses EGF-promoted cell migration by decoupling EGFR activity from vesicular recycling. Sci. Signal *11*. https://doi.org/10.1126/scisignal.aat0114.

Subbarayal, P., Karunakaran, K., Winkler, A.C., Rother, M., Gonzalez, E., Meyer, T.F., and Rudel, T. (2015). EphrinA2 receptor (EphA2) is an invasion and intracellular signaling receptor for Chlamydia trachomatis. PLoS Pathog *11*, e1004846. https://doi.org/10.1371/journal.ppat.1004846.

Tandon, M., Vemula, S.V., and Mittal, S.K. (2011). Emerging strategies for EphA2 receptor targeting for cancer therapeutics. Expert Opin. Ther. Targets *15*, 31–51. https://doi.org/10.1517/14728222.2011.538682.

Tonge, P.J. (2018). Drug-target kinetics in drug discovery. ACS Chem. Neurosci. *9*, 29–39. https://doi.org/10.1021/acschemneuro.7b00185.

Trenker, R., and Jura, N. (2020). Receptor tyrosine kinase activation: from the ligand perspective. Curr. Opin. Cell Biol. *63*, 174–185. https://doi.org/10.1016/j.ceb.2020.01.016.

Vauquelin, G., and Charlton, S.J. (2013). Exploring avidity: understanding the potential gains in functional affinity and target residence time of bivalent and heterobivalent ligands. Br. J. Pharmacol. *168*, 1771–1785. https://doi.org/10.1111/bph.12106.

Verheyen, T., Fang, T., Lindenhofer, D., Wang, Y., Akopyan, K., Lindqvist, A., Hogberg, B., and Teixeira, A.I. (2020). Spatial organization-dependent EphA2 transcriptional responses revealed by ligand nanocalipers. Nucleic Acids Research *48*, 5777–5787. https://doi.org/10.1093/nar/gkaa274.

Wakayama, Y., Miura, K., Sabe, H., and Mochizuki, N. (2011). EphrinA1-EphA2 signal induces compaction and polarization of madin-darby canine kidney cells by inactivating ezrin through negative regulation of RhoA. J. Biol. Chem. *286*, 44243–44253. https://doi.org/10.1074/jbc.M111.267047.

Walker-Daniels, J., Riese, D.J., 2nd, and Kinch, M.S. (2002). c-Cbl-Dependent EphA2 protein degradation is induced by ligand binding. Mol. Cancer Res. *1*, 79–87.

Wang, S., Placzek, W.J., Stebbins, J.L., Mitra, S., Noberini, R., Koolpe, M., Zhang, Z., Dahl, R., Pasquale, E.B., and Pellecchia, M. (2012). Novel targeted system to deliver chemotherapeutic drugs to EphA2-expressing cancer cells. J. Med. Chem. *55*, 2427–2436. https://doi.org/10.1021/jm201743s.

Watson, J., Arey, B.J., and Alt, A. (2014). Biasing receptor tyrosine kinase signaling pathways. In

Biased Signaling in Physiology, Pharmacology and Therapeutics, B.J. Arey, ed. (Elsevier Inc.), pp. 137–172.

Wilson, K., Shiuan, E., and Brantley-Sieders, D.M. (2021). Oncogenic functions and therapeutic targeting of EphA2 in cancer. Oncogene *40*, 2483–2495. https://doi.org/10.1038/s41388-021-01714-8.

Wilson, K.J., Gilmore, J.L., Foley, J., Lemmon, M.A., and Riese, D.J., 2nd (2009). Functional selectivity of EGF family peptide growth factors: implications for cancer. Pharmacol. Ther. *122*, 1–8. https://doi.org/10.1016/j.pharmthera.2008.11.008.

Xu, Q., Lin, W.C., Petit, R.S., and Groves, J.T. (2011). EphA2 receptor activation by monomeric Ephrin-A1 on supported membranes. Biophysical J. *101*, 2731–2739. https://doi.org/10.1016/j.bpj.2011.10.039.

Yang, N.Y., Fernandez, C., Richter, M., Xiao, Z., Valencia, F., Tice, D.A., and Pasquale, E.B. (2011). Crosstalk of the EphA2 receptor with a serine/threonine phosphatase suppresses the Akt-mTORC1 pathway in cancer cells. Cell Signal *23*, 201–212. https://doi.org/10.1016/j.cellsig.2010.09.004.

Zhang, T., Hua, R., Xiao, W., Burdon, K.P., Bhattacharya, S.S., Craig, J.E., Shang, D., Zhao, X., Mackey, D.A., Moore, A.T., et al. (2009). Mutations of the EPHA2 receptor tyrosine kinase gene cause autosomal dominant congenital cataract. Hum. Mutat. *30*, E603–E611. https://doi.org/10.1002/humu.20995.

Zhou, N., Zhao, W.D., Liu, D.X., Liang, Y., Fang, W.G., Li, B., and Chen, Y.H. (2011). Inactivation of EphA2 promotes tight junction formation and impairs angiogenesis in brain endothelial cells. Microvasc. Res. *82*, 113–121. https://doi.org/10.1016/j.mvr.2011.06.005.

Zisch, A.H., and Pasquale, E.B. (1997). The Eph family: a multitude of receptors that mediate cell recognition signals. Cell Tissue Res. *290*, 217–226. https://doi.org/10.1007/s004410050926.

STAR★METHODS

KEY RESOURCES TABLE

REAGENT or RESOURCE	SOURCE	IDENTIFIER
Antibodies		
EphA2 pY588	Cell Signaling	#12677; RRID: AB_2797989
EphA2 pY772	Cell Signaling	#8244; RRID: AB_10860415
EphA2 pY930	ThermoFisher/Invitrogen	#PA5-64784; RRID: AB_2663147
EphA2	Cell Signaling	#6997; RRID: AB_10827743
AKT pS473	Cell Signaling	#4060; RRID: AB_2315049
AKT	Cell Signaling	#9272; RRID: AB_329827
HRP-conjugated anti-phosphotyrosine (P-Tyr-100)	Cell Signaling	#5465; RRID: AB_10694719
HRP-conjugated anti-rabbit secondary	ThermoFisher/Invitrogen	#A16110; RRID: AB_2534782
Chemicals, peptides, and recombinant proteins		
EphA2 Fc	R&D Systems	#639-A2
Fc	MP Biomedicals	#55911
ephrinA1-Fc	R&D Systems	#602-A1-200
EphA receptor Fc fusions	R&D Systems	#SMPK1
EphB receptor Fc fusions	R&D Systems	#SMPK2
ephrinA5 AP	Gomez-Soler et al., 2019	N/A
ephrinB2 AP	Gomez-Soler et al., 2019	N/A
Peptides	GenScript	Custom, see Figure 1 and Tables S1, S2
Experimental models: Cell lines		
PC3	ATCC	#CRL-1435
HEK293-AD	Cell Biolabs	#AD-100
HEK293T	ATCC	#CRL-3216
Recombinant DNA		
EphA2-EYFP in pcDNA3	Singh et al., 2018	N/A
EphA2-mTURQ in pcDNA3	Singh et al., 2018	N/A
EphA2 G131Y-EYFP in pcDNA3	Singh et al., 2018	N/A
EphA2 G131Y-mTURQ in pcDNA3	Singh et al., 2018	N/A
EphA2 L223R/L254R/V255R-EYFP in pcDNA3	Singh et al., 2018	N/A
EphA2 L223R/L254R/V255R-mTURQ in pcDNA3	Singh et al., 2018	N/A
EGFP in pLVX-IRES-Neo	Barquilla et al., 2016	N/A
FLAG-EphA2 WT in pLVX-IRES-Neo	Barquilla et al., 2016	N/A
FLAG-EphA2 Δjxtm-1 in pLVX-IRES-Neo	This paper	N/A
FLAG-EphA2 Δjxtm-2 in pLVX-IRES-Neo	This paper	N/A
Software and algorithms		
Image J	Schneider et al., 2012	https://imagej.nih.gov/ij/
Prism versions 7,8,9	GraphPad	N/A
MATLAB R2018B	MathWorks	N/A

RESOURCE AVAILABILITY

Lead contact

Further information and requests for reagents should be directed to and will be fulfilled by the lead contact, Dr. Elena Pasquale (elenap@sbpdiscovery.org).

Materials availability

The FLAG-EphA2 Δjxtm-1 and FLAG-EphA2 Δjxtm-2 plasmids generated in this study will be available for academic researchers upon completion of a Material Transfer Agreement. The peptides can be purchased from GenScript or other companies that synthesize custom peptides.

Data and code availability

This study did not generate original code. Any additional information required to reanalyze the data reported in this paper is available from the lead contact upon request.

METHOD DETAILS

Peptide synthesis and design

All the peptides were purchased from GenScript. Peptide identity and purity were verified by GenScript using mass spectrometry and high-performance liquid chromatography (HPLC) (Table S1). Peptide solubility values in PBS, H_2O or DMSO reported in Table S1 were determined by GenScript as previously described (Gomez-Soler et al., 2019). All concentrated peptide stocks were prepared in DMSO and stored frozen in aliquots at –80°C.

To generate more stable dimers without a reducible disulfide bond, we replaced the disulfide bond of dimers (**2**) and (**6**) with a non-reducible covalent bond. To obtain the C-terminally linked dimer, we added a C-terminal lysine to one monomeric moiety and attached the second monomeric moiety to the side chain of this lysine (Lys-linked dimer (**3**) in Figure 1). To obtain the N-terminally linked dimer, we added an N-terminal azido-lysine to one monomeric building block and an N-terminal propargylglycine to the other, so that click chemistry could be used to generate an N-terminal covalent bond (click dimer (**7**) in Figure 1). The potency of dimers (**3**) and (**7**) is very similar to that of the corresponding disulfide-linked dimers (**2**) and (**6**), respectively (Figures 1, 2A, 2B, and 3A).

In silico modeling

Initial models of dimeric peptides bound to two EphA2 LBDs were based on our previous crystal structure of the βA-WLA-YRPK-bio (**17***) peptide (Table S2) in complex with the EphA2 LBD (PDB 6NK1 (Gomez-Soler et al., 2019)). For the model with the C-terminally linked βA-WLA-YGSGC dimer (**1**), we used the peptide as observed in the crystal structure without modifications and linked two peptides by replacing the C-terminal "RPK-biotin" sequence with the "GSG" linker sequence followed by a cysteine to enable disulfide bond formation (Figure 1).

For the model of EphA2 bound to the N-terminally-linked CGA-WLA-YRPK dimer (**5**), we first generate an EphA2 LBD dimer with the ClusPro web server (Kozakov et al., 2017). The peptide was added by overlaying it from our previous EphA2 LBD/βA-WLA-YRPK-bio (**17***) complex structure and replacing the N-terminal βA residue with the CGA sequence (Model 1 in Figure S2B). Further manual adjustments were used to generate N-terminal dimer Model 2 in Figure S2C.

For the model of EphA2 bound to head-to-tail peptide dimer (**8**), we generate an EphA2 LBD dimer with the Frodock web server (Ramirez-Aportela et al., 2016). The peptide was added by overlaying it from our previous EphA2 LBD/βA-WLA-YRPK-bio (**17***) complex structure and the linker sequence (GG) was manually modeled. All peptide-EphA2 dimeric models were subsequently optimized using the FlexPepDock web server (London et al., 2011).

Isothermal titration calorimetry (ITC)

The human EphA2 LBD (residues 28–200) was expressed in *E. coli* and purified as described previously (Gomez-Soler et al., 2019). ITC experiments were performed as described previously (Gomez-Soler et al., 2019) with adjustments to account for the 2:1 EphA2 LBD:dimeric peptide binding mode. Briefly, 2 μL aliquots of

200–250 μM EphA2 LBD were titrated into the cell containing 205 μL of 10–12.5 μM peptide. Each titration was performed twice and individually analyzed.

ELISAs

Inhibition of EphA2-ephrin-A5 binding by peptides was measured as previously described (Gomez-Soler et al., 2019). Briefly, EphA2 Fc (#639-A2, R&D Systems) was immobilized on protein A coated 96-well plates and then incubated with 0.05 nM ephrinA5 alkaline phosphatase (AP) and different peptide concentrations. The amount of bound ephrinA5 AP was quantified by using p-nitrophenyl phosphate substrate (#34045, Pierce-Thermo Scientific) diluted in SEAP buffer (105 mM diethanolamine, 0.5 mM $MgCl_2$, pH 9.8) and optical density at 405 nm (OD_{405}) was measured. OD_{405} from wells coated with Fc alone was subtracted as background. The selectivity of dimeric peptides for EphA2 was determined in a similar assay by measuring inhibition of 0.05 nM ephrinA5 AP binding to different EphA receptor Fc fusion proteins (#SMPK1, R&D Systems) and inhibition of 0.5 nM ephrinB2 AP binding to different EphB receptor Fc fusion proteins (#SMPK2, R&D Systems). Dimeric peptide concentrations corresponding to approximately 100 times the IC_{50} values for inhibition of EphA2-ephrinA5 interaction were used. For ELISA experiments, we used ephrinA5 AP and ephrinB2 AP secreted in the cell culture medium of transiently transfected HEK293 cells. The medium was heated at 60°C for 30 min to inactivate endogenous alkaline phosphatase and the concentration of the ephrin AP fusion protein was measured in an alkaline phosphatase activity assay based on the specific activity reported for alkaline phosphatase of 2U/μg (Cullen, 2000; Flanagan et al., 2000).

EphA2 constructs

The EphA2-EYFP and EphA2-mTURQ constructs in pcDNA3 used for FRET have been previously described (Gomez-Soler et al., 2019). N-terminally FLAG-tagged EphA2 WT in the pLVX-IRES-Neo lentiviral construct and the pLVX-IRES-Neo-EGFP control construct have also been described (Barquilla et al., 2016). The EphA2 ΔQ565-L582 (Δjxtm-1) and ΔQ565-T606 (Δjxtm-2) mutants with deletions in the juxtamembrane segment were generated by overlapping PCR using the pLVX-IRES-Neo FLAG-EphA2 WT construct as the template. All regions amplified by PCR were verified by sequencing.

Immunoblotting

PC3 prostate cancer cells (ATCC, #CRL-1435; authenticated by short tandem repeat analysis) were cultured in RPMI 1640 (ThermoFisher Scientific/Gibco, #11875–093) containing 10% fetal bovine serum with 1% antibiotic-antimycotic solution (Corning, #30-004-Cl), as previously described (Gomez-Soler et al., 2019). HEK293-AD human embryonic kidney cells (Cell Biolabs, #AD-100) (~2.5×10^6) were transfected in 6-well plates with 0.5 ug EphA2 WT and Δjxtm-1 and Δjxtm-2 mutant constructs and selected with G418 (1 mg/mL) for 15 days.

For stimulations with ligands, once the cells reached 70–80% confluence, they were starved in the same medium without serum for 1 h. For dose-response experiments, PC3 cells were treated with different ligand concentrations for 15 min. For time-course experiments, PC3 cells were treated for different times with saturating ligand concentrations: 50 nM ephrinA1-Fc (R&D Systems, #602-A1-200), 1,000 nM dimer (**3**), 100 nM dimer (**7**), 150 nM dimer (**8**) or 30 μM monomer (**10**). HEK293 cells stably transfected with EphA2 WT and mutants were treated for 2.5 min with 40 nM ephrinA1-Fc, 50 nM dimer (**2**), 25 nM dimer (**6**) or 10 nM dimer (**8**). In the experiments in Figure S8, HEK293 cells stably transfected with EphA2 WT were treated with 10 μM LY294002 for 30 min and then with 50 nM dimer (**2**) or 10 nM dimer (**8**) for 5 min.

After treatment with ligands, the cells were rinsed once with cold PBS containing Ca^+ and Mg^+ (Lonza, #17–513F) and collected in Bolt LDS sample buffer (Life Technologies, #B0007) containing 2.5% β-mercaptoethanol. Lysates were heated at 95° for 2 min, briefly sonicated and run on SDS-PAGE gels. After semi-dry transfer using PVDF transfer packs (Bio-Rad, #1704272) with a Trans-Blot Turbo Transfer System (Bio-Rad Laboratories), the immobilon membranes were blocked with 5% BSA in 0.1% Tween-20 in TBS (150 mM NaCl, 50 mM Tris HCl pH 7.5) for 1 h and then incubated in the cold overnight with antibodies from Cell Signaling Technology recognizing EphA2 pY588 (#12677, at 1:2,000 dilution), EphA2 pY772 (#8244, at 1:1,000), EphA2 (#6997 at 1:1,000 dilution), AKT pS473 (#4060, at 1:2,000 dilution) and AKT (#9272, at 1:1,000 dilution) and with an antibody from ThermoFisher Scientific/Invitrogen recognizing EphA2 pY930 (#PA5-64784, at 1:1,000 dilution). After washing, the membranes were incubated with an HRP-conjugated anti-rabbit secondary antibody (Invitrogen anti-rabbit #A16110, at a 1:3,000 dilution). For phosphotyrosine blots, membranes were incubated for 1 h with a phosphotyrosine antibody conjugated to HRP from Cell

Signaling Technology (P-Tyr-100, #5465, at 1:1,000 dilution). The chemiluminescence signal was captured using ChemiDoc Touch Imaging System (Bio-Rad), quantified using Image Lab (Bio-Rad) and analyzed using Prism software (GraphPad).

Cell retraction

For the retraction assay, PC3 cells were plated overnight in RPMI-1640 medium with 10% FBS and penicillin/streptomycin on round coverslips (ThermoFisher, Fisherbrand #12-545-80) in 24-well plates at 24,000 cells/well. The cells were then serum starved for 4 h, and cell retraction was induced at 37°C by stimulation for 10 min with ephrinA1-Fc or peptide ligands. Stocks of peptide ligands were prepared at 500X final concentrations in DMSO so that the final DMSO concentration in the wells was 0.2%. Control cells were treated with 0.2% DMSO without any ligand. In 2 of the 4 experiments 0.2% DMSO was also added to the ephrinA1-Fc wells, which did not seem to affect retraction. The cells were then fixed in 4% paraformaldehyde in PBS for 15 min at RT, permeabilized in 0.5% Triton X-100 in PBS for 5 min, incubated with blocking buffer (3% BSA in PBS) for 30 min, labeled for actin with rhodamine-conjugated phalloidin (Biotium, #00027) diluted in blocking buffer for 1 h. Coverslips were mounted using ProLong™ Gold Antifade mountant containing DAPI to stain nuclei (ThermoFisher/Invitrogen, #P36931). Cell images were captured using an Echo Revolve fluorescence microscope with a 20X objective. Cell areas were measured using ImageJ (National Institutes of Health, Bethesda, MD) and analyzed using Prism (GraphPad).

Analysis of ligand bias

The values for the bias factor β_{lig} (Karl et al., 2020; Rajagopal et al., 2011) reported in Figure 1 were calculated for each ligand using the EC_{50} and E_{top} values in Figure 1, according to:

$$\beta_{lig} = \log\left(\left(\frac{EC_{50,pY588}\ E_{top,pAKTinh}}{EC_{50,pAKTinh}\ E_{top,pY588}}\right)_{lig} - \log\left(\frac{EC_{50,pY588}\ E_{top,pAKTinh}}{EC_{50,pAKTinh}\ E_{top,pY588}}\right)_{ref}\right) \quad \text{(Equation 1)}$$

where ref is the reference ligand, ephrinA1-Fc. The contribution of the different factors (EC_{50} for pY588, EC_{50} for pAKT inhibition, E_{top} for pY588 and E_{top} for pAKT inhibition) to the β_{lig} values varies depending on the ligand (Figure S9).

Förster resonance energy transfer (FRET)

The HEK293T cells used in the FRET experiments were from ATCC (#CRL-3216). The cells were cultured in Dulbecco's Modified Eagle's Medium (DMEM, ThermoFisher, 31,600,034) with 10% fetal bovine serum (FBS, Hyclone, #SH30070.03) at 37°C in the presence of 5% CO_2. FRET experiments were performed as previously described (Gomez-Soler et al., 2019). The cells were co-transfected with different ratios of EphA2-mTURQ DNA and EphA2-EYFP. Co-transfected dishes contained a total of 2 μg DNA, with varying donor (EphA2-mTURQ) to acceptor (EphA2-EYFP) ratios. Twenty-four hours after transfection, the cells were starved in the same medium for 12 hprior to imaging (King et al., 2016).

Integrated fluorescence images were obtained in the presence or in the absence of 2 μM βA-WLA-YRPKC dimer (**2**) or CGA-WLA-YRPK dimer (**5**) using a two-photon microscope. For each cell, two microscope scans were acquired – an acceptor excitation scan at λ = 960 nm (to measure acceptor fluorescence) and a donor excitation scan at λ = 840 nm (to measure both donor and sensitized acceptor fluorescence) (Gomez-Soler et al., 2019). The FSI-FRET method was used to measure FRET efficiency, donor concentration, and acceptor concentration in micron-sized regions of the plasma membrane. To convert pixel level intensities of the images to concentrations, calibration solutions of purified fluorescent proteins were used. A detailed description of the FSI-FRET methodology has been published (King et al., 2017). The raw FRET data are shown in Figure S7A.

The fitting procedure and the analysis that differentiates between dimers and higher order oligomers have been described in detail in published work (King et al., 2017). The FRET data are interpreted within the context of thermodynamic models that are built for different types of oligomerization (with oligomer order = n) and fitted to the data to calculate the mean squared error (MSE; Figure S7B). Extensive evaluation of this approach has shown that an MSE minimum at n = 2 reliably identifies dimer populations (King et al., 2017). An MSE minimum at n > 2 or the same MSE value for different oligomer orders points to the presence of oligomers larger than dimers, although the presence of dimers cannot be excluded (King et al., 2017). While the exact order of the oligomers (n = 3, 4, 5, etc.) cannot be determined from this analysis, we

have shown that the method reliably gives the receptor fraction that exists in an oligomeric state (i.e. dimers or higher order oligomers/clusters) (King et al., 2017).

QUANTIFICATION AND STATISTICAL ANALYSIS

Statistical analyses were performed using Prism software versions 7, 8 or 9 (GraphPad Software Inc., San Diego, CA). Statistical details of experiments can be found in the figure legends, including the statistical tests used, p values, the definitions of n, and whether averages and SD or averages and SEM are reported/shown.